

Quartzite Complexities: Non-destructive analysis of bifacial points from Västerbotten, Sweden

September 13, 2023

Northern Fennoscandia represents a geologically complex region affected by both glacial and postglacial processes. Quartzite was a key material type utilized by hunter-gatherers in Northern Sweden around the period 4 000 – 2 000 BP, and is thus critical to the understanding of raw material procurement and material flow within the region. However, there is a severe lack of methodological development in the characterization of these materials, and provenance of locally available geological material is complex and fraught with uncertainty. 126 points and preforms made from quartz/quartzite were sampled from 47 archaeological sites along the upper Ångerman river valley in Västerbotten, Sweden. The material has been analysed non-destructively using three separate portable spectroscopic instrumentations (Near-infrared, Raman, X-Ray Fluorescence). Evaluation of the spectra and exploratory data analysis using Principal Component Analysis demonstrates detectable differences in the material that likely stem from diagenetic/paragenetic origin. The presence of graphite, muscovite and biotite could likewise provide information on the material's metamorphic grade. In addition to reaffirming the potential of field-based screening instrumentation, these results will benefit future surveys of geological sources in the region. They also indicate potential for the construction of a predictive model that could classify the quartzite based on its chemical characteristic. Such a model would prove useful in future spatial analysis and testing of models of raw material management.

¹ Environmental Archaeology Lab, Department of Historical, Philosophical and Religious studies, Umeå University, Umeå, Sweden

² Department of Forest Biomaterials and Technology, Swedish University of Agricultural Sciences, Umeå, Sweden

* Correspondence: [Mattias Sjölander <mattias.sjolander@mumu.se>](mailto:Mattias.Sjolander@mumu.se)

Keywords: Hunter-Gatherer; Lithics; Provenance; Quartzite; Vibrational spectroscopy; Scandinavia

Introduction

Petrographic characterization and provenance studies are instrumental for inferring trade and exchange among prehistoric societies (Tykot, 2003). The presence of lithic material foreign to the

local region of an archaeological site, raises important questions on the processes that resulted in its eventual deposition and discovery. The characterization of geological material and identification of geological sources are the first steps in reconstructing a prehistoric community's strategies for raw material selection and management. Flint and obsidian have been central to studies of trade and exchange in European prehistory, due in part to the well-surveyed geological sources for these materials (Tykot, 2017). This focus has led to a bias which has been highlighted by Prieto et al. (2019: 15). Recent decades, however, have seen an increase in interest for non-flint lithics and raw material studies (Blomme et al., 2012; Dalpra and Pitblado, 2016; Prieto et al., 2021, 2020; Prieto et al., 2019; Ramacciotti et al., 2019).

In Northern Sweden, quartz and quartzite dominate the lithic assemblages and have been used in settlement, exchange and mobility studies (Baudou, 1978). Models have been proposed for raw material sourcing and trade and exchange for the less common slate and flint finds within Northern Sweden (Halén, 1994: 115-122; Lundberg, 1997: 161-171). There has, however, been little development in the petrographic characterization and provenance study of quartz and quartzite (Broadbent, 1979; Callahan et al., 1992; Knutsson et al., 2016; Tallavaara et al., 2010). A possible reason for this might well be the complex geological background of the region (Bargel, 2003; Stephens and Bergman Weiher, 2020; Stroeven et al., 2016). Northern Sweden is extensively covered by glacial till, and whilst there are identifiable source areas (e.g. small bedrock quarries), there is an extremely large number of other potential sources of raw materials to be found in moraine deposits. The few existing theories on lithic material sourcing within the North Swedish region describe strategies for direct procurement from the mountain zone (2012, 1985). This does not, however, account for the possibility that the material was sourced locally around the site, as part of an embedded adaptation strategy (Binford, 1979; Rankama et al., 2006: 249-250). A new approach to provenance studies is therefore required in this region.

Prieto et al. (2019: 15; 2020: 32) note the ambiguous usage of the term quartzite in archaeology, with it often being used interchangeably between sedimentary orthoquartzite and metamorphic quartzite. When defining quartzite, different researchers have emphasised different features as being characteristics of the material (Howard, 2005). Visual characterization with the naked eye is typically unreliable, and microscopic analysis is recommended for the identification of metamorphic structures. The need for field-based methodologies is, however, stressed by Howard (2005: 708). Spectroscopic surface measurements are fast and can be adapted for use in the field. However, artefact collections (museum, private, etc.) also represent a valuable resource and asset, with easy access to large potential datasets with a wide geographical distribution. Destructive analysis on material from these collections, which are often unique and include sensitive cultural heritage material, are not always suitable or permitted, and thus there is a clear need for the development and testing of non-destructive techniques such as those presented in this study.

In this study, three different spectroscopic techniques have been applied to material stored in collections at Västerbottens museum in Umeå, Sweden (<https://samlingar.vbm.se/>). X-Ray Fluorescence (XRF) is a well-established spectroscopic technique for petrographic characterization (Shackley, 2011a; Tykot, 2003), due to its capability of providing element compositional data. The use of near-infrared spectroscopy (NIRS) is similarly well-known, as described by Norris (1996), and there is a large body of work dedicated to the fingerprinting of geological materials (Clark et al., 1990; Hunt, 1977; Linderholm and Geladi, 2014a, 2014b; Sciuto, 2018). Complementary to NIR, Raman spectroscopy has been applied extensively in both the Cultural Heritage sector, in the analysis of artwork and manuscripts, and the Earth sciences (Dubessy et al., 2012).

The geological complexity of both the region and the material necessitates new approaches to studies of both raw materials and artefact distributions. This paper presents an assessment of the potential for non-destructive spectroscopy to advance the characterization of quartz and quartzite material without the use of references from known geological sources. The currently available data on the chemical characteristic of quartz and quartzite in this region of Northern Sweden are limited, however, and thus this aims to:

- Assess the potential of multispectral non-destructive analysis of quartzite using NIRS, Raman and ED-XRF
- Assess the variability, and identify features, in quartzite that may be of use in its characterization
- Discuss the implications of these methods for developing future strategies for studying raw material management of quartzite between 4 000 and 2 000 BP in Northern Sweden

Material

This study includes spectroscopic surface measurements collected on bifacial points (probable arrowheads and spear points) made of, what has been classified by archaeologists as, *brecciated quartz* and quartzite. The points have been recovered from archaeological sites during excavations and surveys, including stray finds, in Västerbotten County, Sweden (Fig. 1 & Table 1). The sites are distributed along the Ångerman river valley, from Lake Kultsjön in the north, towards the town of Åsele in the south. The dataset consists of 126 points, point fragments and preforms stored in the collections at Västerbottens museum (www.vbm.se) and have been analysed using NIRS, Raman scattering and ED-XRF (Fig. 2; Fig. 3).

The geographically closest chronology for bifacial points is centred around southeast Norway (Mjærum, 2012), but a few attempts have been made for Northern Sweden (Baudou, 1992: 99; Forsberg, 1985: 5; Forsberg, 1989). The latter suggest a period of use between ca. 3 800 – 2 000 BP (Käck, 2009: 60). Studies of raw material use at sites dating to this period seem to indicate an increase in the use of quartzite when compared to earlier periods (Baudou, 1978).

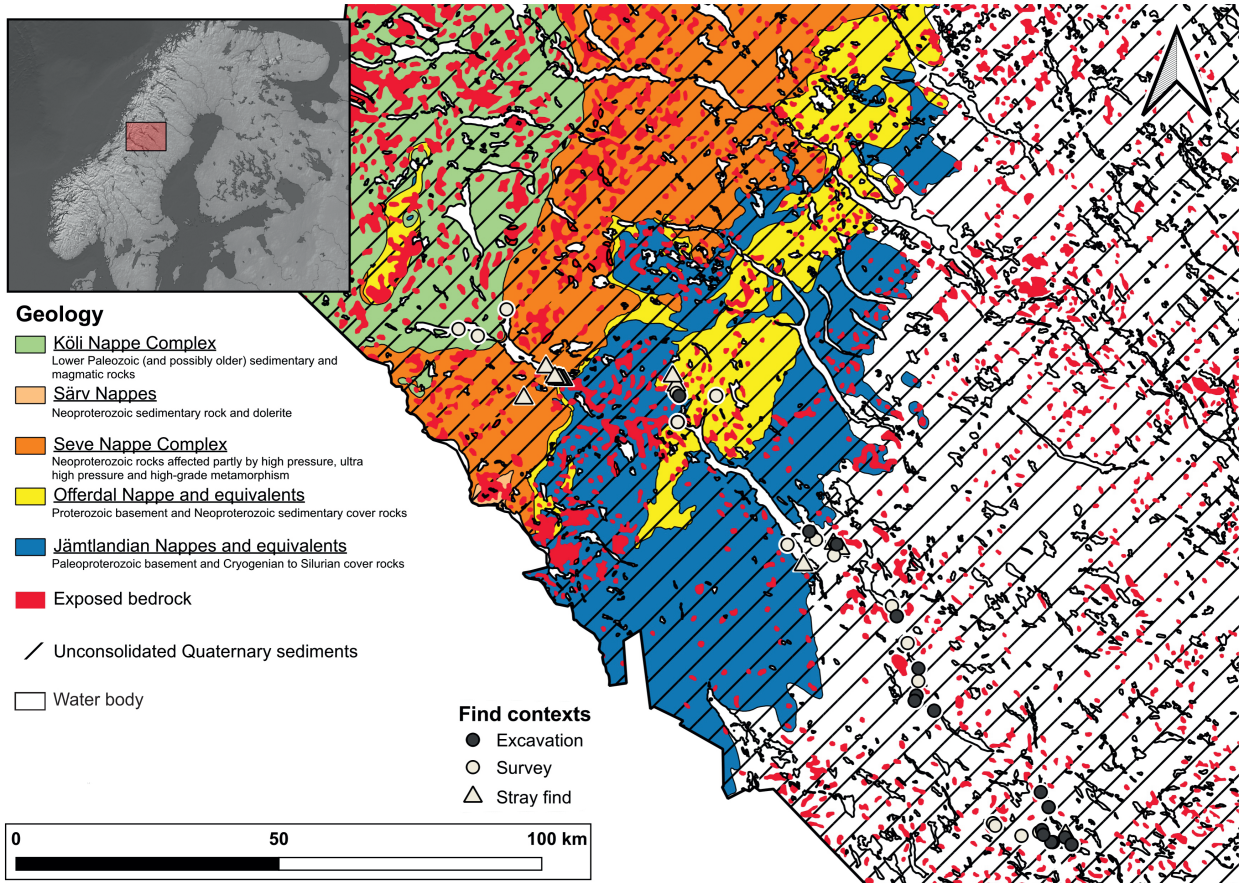


Fig. 1: Geographical distribution of the sampled sites, with find context, along the river of Ångermanälven, Västerbotten, Sweden. The Late Quaternary reincorporation of geological material from the Scandian mountains into the sediments in the forest inlands adds to the complexity of questions of provenance. Tectonic symbology after (Gee and Stephens 2020). Made with © Sveriges Geologiska Undersökning, Lantmäteriet (CC0), Natural Earth, and Riksantikvarieämbetet.

Table 1: List of artefact location, material and type.

Sample ID	Site	Latitude	Longitude	Parish	Material	Find context
410	Vilhelmina 1069	65.09	15.18	Vilhelmina	Quartzite	Survey
400	Vilhelmina 109	64.97	15.37	Vilhelmina	Quartzite	Stray find
431	Vilhelmina 112	64.93	15.25	Vilhelmina	Quartzite	Stray find
411	Vilhelmina 1124	65.04	15.06	Vilhelmina	Quartzite	Survey
417	Vilhelmina 1127	65.05	14.98	Vilhelmina	Quartzite	Survey

Sample ID	Site	Latitude	Longitude	Parish	Material	Find context
265	Vilhelmina 114	64.97	15.38	Vilhelmina	Quartzite	Stray find
272	Vilhelmina 114	64.97	15.38	Vilhelmina	Quartzite	Stray find
241	Vilhelmina 115	64.97	15.39	Vilhelmina	Quartzite	Stray find
244	Vilhelmina 115	64.97	15.39	Vilhelmina	Quartzite	Stray find
249	Vilhelmina 115	64.97	15.39	Vilhelmina	Quartzite	Stray find
258	Vilhelmina 115	64.97	15.39	Vilhelmina	Quartzite	Stray find
267	Vilhelmina 115	64.97	15.39	Vilhelmina	Quartzite	Stray find
269	Vilhelmina 115	64.97	15.39	Vilhelmina	Quartzite	Stray find
377	Vilhelmina 115	64.97	15.39	Vilhelmina	Quartzite	Stray find
390	Vilhelmina 115	64.97	15.39	Vilhelmina	Quartzite	Stray find
391	Vilhelmina 115	64.97	15.39	Vilhelmina	Quartzite	Stray find
393	Vilhelmina 115	64.97	15.39	Vilhelmina	Quartzite	Stray find
246	Vilhelmina 117	64.97	15.39	Vilhelmina	Quartzite	Stray find
259	Vilhelmina 117	64.97	15.39	Vilhelmina	Quartzite	Stray find
262	Vilhelmina 117	64.97	15.39	Vilhelmina	Quartzite	Stray find
280	Vilhelmina 117	64.97	15.39	Vilhelmina	Quartzite	Stray find
392	Vilhelmina 117	64.97	15.39	Vilhelmina	Quartzite	Stray find
245	Vilhelmina 118	64.97	15.41	Vilhelmina	Quartzite	Stray find
255	Vilhelmina 118	64.97	15.41	Vilhelmina	Quartzite	Stray find
260	Vilhelmina 118	64.97	15.41	Vilhelmina	Quartzite	Stray find
261	Vilhelmina 118	64.97	15.41	Vilhelmina	Quartzite	Stray find
229	Vilhelmina 1254	64.68	16.48	Vilhelmina	Quartzite	Survey
231	Vilhelmina 1254	64.68	16.48	Vilhelmina	Quartzite	Survey
232	Vilhelmina 1254	64.68	16.48	Vilhelmina	Quartzite	Survey
233	Vilhelmina 1254	64.68	16.48	Vilhelmina	Quartzite	Survey
234	Vilhelmina 1254	64.68	16.48	Vilhelmina	Quartzite	Survey
236	Vilhelmina 1254	64.68	16.48	Vilhelmina	Quartzite	Survey
237	Vilhelmina 1254	64.68	16.48	Vilhelmina	Quartzite	Survey
238	Vilhelmina 1254	64.68	16.48	Vilhelmina	Quartzite	Survey

Sample ID	Site	Latitude	Longitude	Parish	Material	Find context
405	Vilhelmina 216	64.68	16.29	Vilhelmina	Quartzite	Survey
268	Vilhelmina 235	64.70	16.38	Vilhelmina	Quartzite	Excavation
195	Vilhelmina 240	64.69	16.40	Vilhelmina	Brecciated quartz	Stray find
235	Vilhelmina 240	64.69	16.40	Vilhelmina	Quartzite	Stray find
406	Vilhelmina 245	64.69	16.41	Vilhelmina	Quartzite	Survey
283	Vilhelmina 252	64.64	16.36	Vilhelmina	Quartzite	Stray find
284	Vilhelmina 252	64.64	16.36	Vilhelmina	Quartzite	Stray find
282	Vilhelmina 263	64.68	16.48	Vilhelmina	Quartzite	Stray find
430	Vilhelmina 335	64.44	16.80	Vilhelmina	Quartzite	Survey
251	Vilhelmina 356	64.67	16.51	Vilhelmina	Quartzite	Stray find
253	Vilhelmina 356	64.67	16.51	Vilhelmina	Quartzite	Stray find
254	Vilhelmina 356	64.67	16.51	Vilhelmina	Quartzite	Stray find
278	Vilhelmina 356	64.67	16.51	Vilhelmina	Quartzite	Stray find
281	Vilhelmina 356	64.67	16.51	Vilhelmina	Quartzite	Stray find
387	Vilhelmina 399	64.55	16.72	Vilhelmina	Quartzite	Excavation
388	Vilhelmina 399	64.55	16.72	Vilhelmina	Quartzite	Excavation
394	Vilhelmina 399	64.55	16.72	Vilhelmina	Quartzite	Excavation
432	Vilhelmina 399	64.55	16.72	Vilhelmina	Quartzite	Excavation
407	Vilhelmina 411	64.51	16.76	Vilhelmina	Quartzite	Survey
429	Vilhelmina 419	64.46	16.80	Vilhelmina	Quartzite	Excavation
386	Vilhelmina 439	64.41	16.78	Vilhelmina	Quartzite	Excavation
403	Vilhelmina 439	64.41	16.78	Vilhelmina	Quartzite	Excavation
359	Vilhelmina 444	64.42	16.79	Vilhelmina	Quartzite	Excavation
378	Vilhelmina 444	64.42	16.79	Vilhelmina	Quartzite	Excavation
384	Vilhelmina 444	64.42	16.79	Vilhelmina	Quartzite	Excavation
385	Vilhelmina 444	64.42	16.79	Vilhelmina	Quartzite	Excavation
401	Vilhelmina 444	64.42	16.79	Vilhelmina	Quartzite	Excavation
402	Vilhelmina 444	64.42	16.79	Vilhelmina	Quartzite	Excavation
397	Vilhelmina 450	64.39	16.86	Vilhelmina	Quartzite	Excavation

Sample ID	Site	Latitude	Longitude	Parish	Material	Find context
404	Vilhelmina 450	64.39	16.86	Vilhelmina	Quartzite	Excavation
227	Vilhelmina 539	64.66	16.48	Vilhelmina	Quartzite	Survey
207	Vilhelmina 542	64.68	16.49	Vilhelmina	Quartzite	Excavation
200	Vilhelmina 611	64.95	15.86	Vilhelmina	Quartzite	Stray find
193	Vilhelmina 619	64.97	15.85	Vilhelmina	Quartzite	Stray find
194	Vilhelmina 619	64.97	15.85	Vilhelmina	Quartzite	Stray find
204	Vilhelmina 619	64.97	15.85	Vilhelmina	Quartzite	Stray find
210	Vilhelmina 619	64.97	15.85	Vilhelmina	Quartzite	Stray find
214	Vilhelmina 619	64.97	15.85	Vilhelmina	Quartzite	Stray find
215	Vilhelmina 619	64.97	15.85	Vilhelmina	Quartzite	Stray find
201	Vilhelmina 636	64.94	15.87	Vilhelmina	Quartzite	Excavation
208	Vilhelmina 636	64.94	15.87	Vilhelmina	Quartzite	Excavation
212	Vilhelmina 636	64.94	15.87	Vilhelmina	Quartzite	Excavation
221	Vilhelmina 636	64.94	15.87	Vilhelmina	Quartzite	Excavation
413	Vilhelmina 637	64.94	15.86	Vilhelmina	Quartzite	Survey
196	Vilhelmina 643	64.89	15.86	Vilhelmina	Quartzite	Survey
197	Vilhelmina 643	64.89	15.86	Vilhelmina	Quartzite	Survey
198	Vilhelmina 643	64.89	15.86	Vilhelmina	Quartzite	Survey
213	Vilhelmina 643	64.89	15.86	Vilhelmina	Quartzite	Survey
216	Vilhelmina 643	64.89	15.86	Vilhelmina	Quartzite	Survey
414	Vilhelmina 643	64.89	15.86	Vilhelmina	Quartzite	Survey
415	Vilhelmina 643	64.89	15.86	Vilhelmina	Quartzite	Survey
416	Vilhelmina 643	64.89	15.86	Vilhelmina	Quartzite	Survey
408	Vilhelmina 769	64.57	16.70	Vilhelmina	Quartzite	Survey
230	Vilhelmina 949	64.94	16.02	Vilhelmina	Brecciated quartz	Survey
264	Vilhelmina 95	64.99	15.34	Vilhelmina	Quartzite	Stray find
184	Åsele 101	64.18	17.26	Åsele	Quartzite	Survey
185	Åsele 107	64.17	17.27	Åsele	Quartzite	Excavation
186	Åsele 107	64.17	17.27	Åsele	Quartzite	Survey

Sample ID	Site	Latitude	Longitude	Parish	Material	Find context
187	Åsele 107	64.17	17.27	Åsele	Quartzite	Survey
54	Åsele 115	64.17	17.36	Åsele	Quartzite	Stray find
55	Åsele 115	64.17	17.36	Åsele	Quartzite	Stray find
56	Åsele 115	64.17	17.36	Åsele	Quartzite	Stray find
57	Åsele 115	64.17	17.36	Åsele	Quartzite	Stray find
58	Åsele 115	64.17	17.36	Åsele	Quartzite	Stray find
188	Åsele 117	64.22	17.30	Åsele	Quartzite	Excavation
189	Åsele 117	64.22	17.30	Åsele	Quartzite	Excavation
191	Åsele 117	64.22	17.30	Åsele	Quartzite	Excavation
190	Åsele 119	64.25	17.27	Åsele	Quartzite	Excavation
168	Åsele 129	64.15	17.38	Åsele	Quartzite	Excavation
169	Åsele 129	64.15	17.38	Åsele	Quartzite	Excavation
170	Åsele 129	64.15	17.38	Åsele	Quartzite	Excavation
171	Åsele 129	64.15	17.38	Åsele	Quartzite	Excavation
172	Åsele 129	64.15	17.38	Åsele	Quartzite	Excavation
173	Åsele 129	64.15	17.38	Åsele	Brecciated quartz	Excavation
174	Åsele 129	64.15	17.38	Åsele	Quartzite	Excavation
175	Åsele 129	64.15	17.38	Åsele	Quartzite	Excavation
176	Åsele 129	64.15	17.38	Åsele	Quartzite	Excavation
177	Åsele 129	64.15	17.38	Åsele	Quartzite	Excavation
152	Åsele 182	64.20	17.08	Åsele	Quartzite	Survey
153	Åsele 182	64.20	17.08	Åsele	Quartzite	Survey
424	Åsele 182	64.20	17.08	Åsele	Quartzite	Survey
425	Åsele 182	64.20	17.08	Åsele	Quartzite	Survey
428	Åsele 188	64.19	17.08	Åsele	Quartzite	Survey
167	Åsele 393	64.17	17.36	Åsele	Quartzite	Excavation
426	Åsele 56	64.17	17.19	Åsele	Quartzite	Survey
427	Åsele 56	64.17	17.19	Åsele	Quartzite	Survey
178	Åsele 91	64.16	17.31	Åsele	Quartzite	Survey

Sample ID	Site	Latitude	Longitude	Parish	Material	Find context
179	Åsele 91	64.16	17.31	Åsele	Brecciated quartz	Survey
180	Åsele 91	64.16	17.31	Åsele	Quartzite	Excavation
181	Åsele 92	64.16	17.30	Åsele	Quartzite	Excavation
182	Åsele 99	64.18	17.27	Åsele	Quartzite	Excavation
183	Åsele 99	64.18	17.27	Åsele	Quartzite	Excavation

The dataset includes two main groups of petrographic material, as classified by archaeologists: quartzite and *brecciated quartz* (Swe. “*brecciekvarts*”) (Fig. 2; Table 1). Geological definitions of quartzite include characteristics such as the material being exceptionally hard, predominantly consisting of quartz, and with conchoidal fracturing (Howard, 2005; Prieto et al., 2019; Skolnick, 1965). A reliable classification would thus be based on a combination of chemical and physical (macroscopic and microscopic) properties. Archaeologists, however, tend to classify the material in the field on the basis of visual characteristics and perceived hardness. This can lead to considerable ambiguity, but in general, a material will be archaeologically classified as quartzite in Northern Sweden if it is an exceptionally hard, fine-grained, quartz-rich rock.

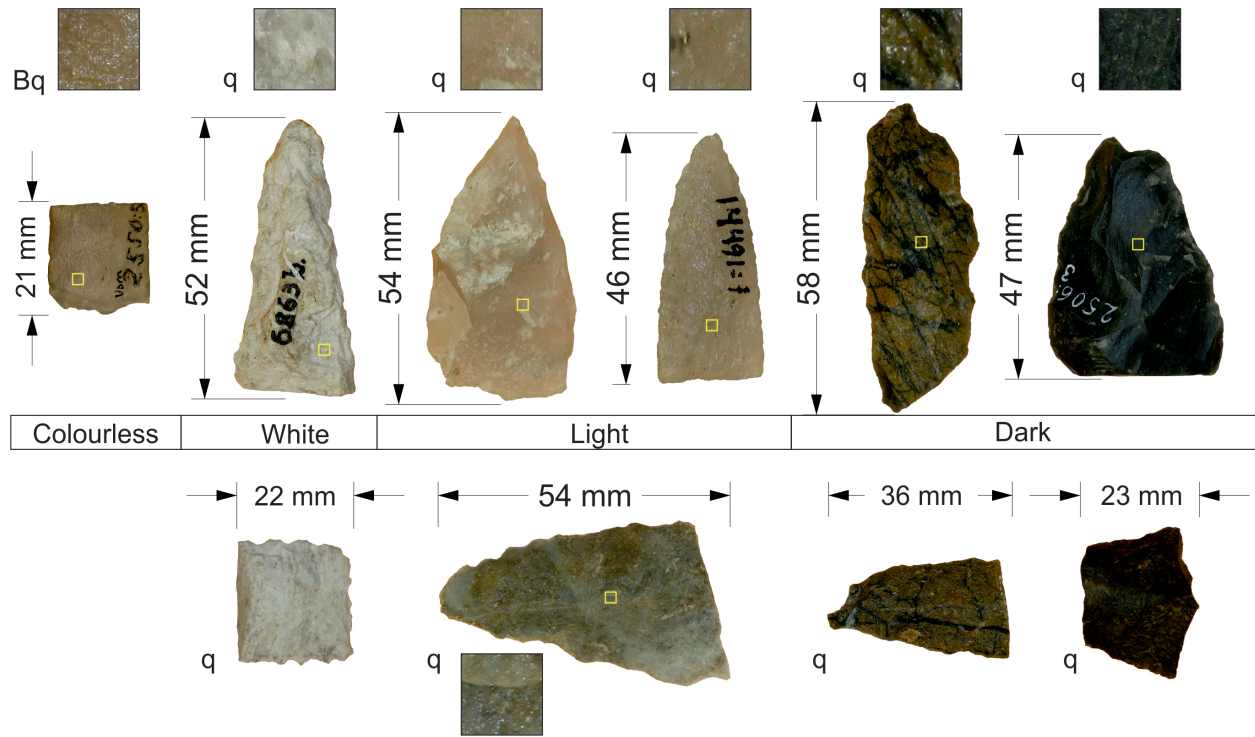


Fig. 2: Examples of the bifacial points studied. The material is heterogeneous in terms of colour, and the surface of the artefacts themselves is not uniform. Ranging from near perfect points to rough preforms, it can be difficult to sample due to light scattering effects and saturation. Length varies between 12 – 138 mm, width between 8 – 67 mm, and thickness between 3 – 76 mm

This study includes 122 and 4 *brecciated quartz* samples. The inclusion of *brecciated quartz* in the study enables the separation of quartz from quartzite, based on non-destructive analysis of their chemical and structural characteristics, to be evaluated. The term *brecciated quartz* (also referred to as *mylonite quartz*) was introduced to archaeologists in Northern Sweden by the geologist Åhman (1967: 8) in his analysis of the petrographic material in the *Early Norrland* project (Åhman, 1967; Biörnstad, 1968). Åhman describes the material as easily mistaken for an unusually pure quartzite, but where the fragmented configuration of the quartz can be identified via microscopic analysis. No detailed information on these microscopic features were mentioned in his original publication. *Brecciated quartz* in particular became a common term used in North Swedish archaeology, and has typically been used to identify a certain translucent type of fine-grained, quartz-rich material that functionally behaves similarly to quartzite (e.g. Holm, 1991: 24) (Fig. 2). As the material frequently has been characterized on the basis of macroscopic characteristics, despite the fundamental features necessary for characterization being microscopic, there is value in including this material as a test group in the study.

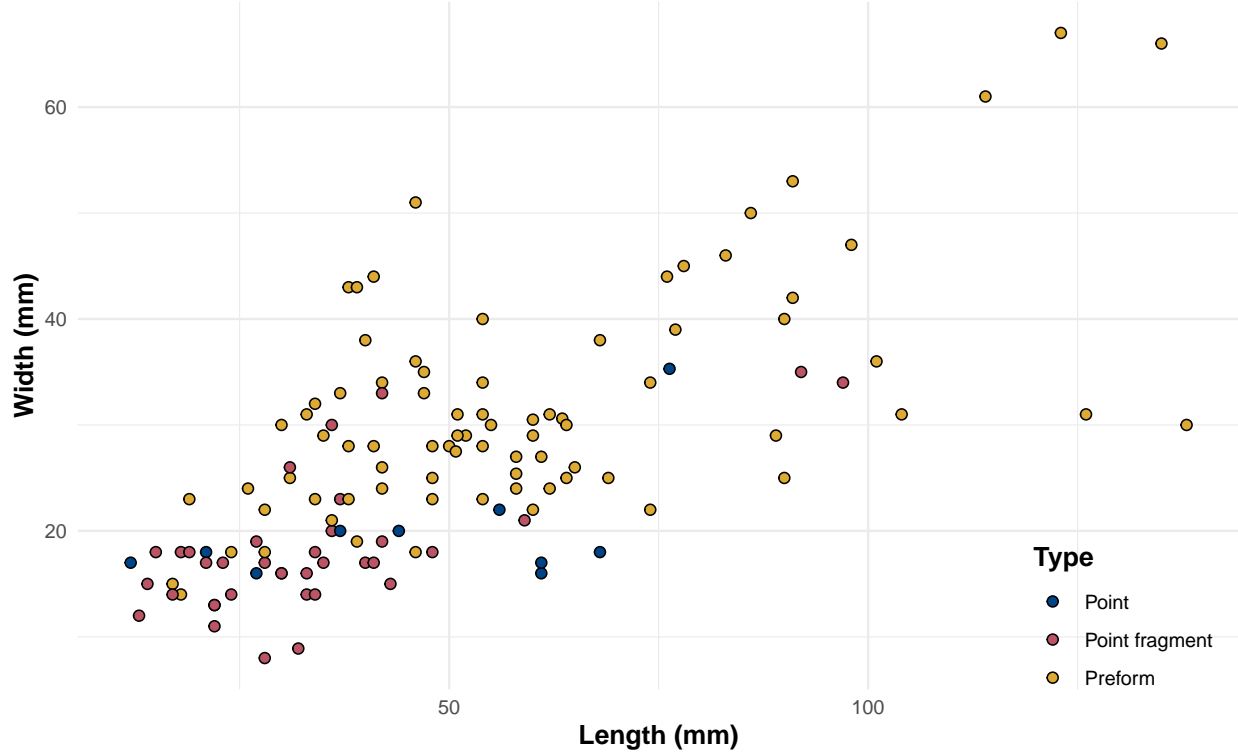


Fig. 3: Scatter plot of length and width measurements (mm) for the sampled artefacts. 8 artefacts have no recorded thickness, which ranges between 3-76 mm. Note that the term point does not differentiate between spear points or arrowheads

Methods

All measurements were collected at the Environmental Archaeology Lab at Umeå University (www.umu.se/en/research/infrastructure/mal/). The analysis was conducted in a dark room in order to minimize stray light, with the main light sources in the room being 2 computer screens. The sampled material is heterogeneous in colour and shape (Fig. 2 - Fig. 3) (see supplementary data). The artefacts range from small and flat point fragments, to large and rough preforms. This variation led to scattering effects and saturation which at times made signal integration difficult.

For NIR and Raman analyses, each artefact was sampled twice, on different sides, with additional measurements where sampling was difficult. When sampling, the probe was positioned in contact with as flat a surface as possible of the artefact. If the material featured high heterogeneity, the sample point was focused on the surrounding matrix, avoiding deviating inclusions (e.g. the dark mineral veins in Fig. 3).

For XRF, the more time-consuming nature of the measurement process necessitated only one measurement per object. The representativeness of the XRF analysis is thus lower, and inferences derived from the results in this study should be used with caution. The risk of misinterpretation is, however, somewhat compensated for by the large size of the dataset, with larger sites including multiple objects that may come from the same geological source. The results from sites with smaller assemblages are, however, more liable to be affected by the limited range of material analysed.

In colour, the artefacts exhibit a mainly black or grey hue, with a subset of semi-translucent material with a beige tint, with some being almost fully translucent. While the colour of the material has been classified according to the Munsell system (see supplementary data), for visualization purposes they have also been sorted into general hues: *dark* (~ N1-N4), *light* (~ N5-N8), *white* (~ N9), and *colourless* (lack of colour, opaque to translucent). In the case of heterogeneous objects the Munsell colour and general hue describes the surrounding matrix.

Instrumentation and data pre-processing

Near Infrared Spectroscopy (NIRS)

On the basis of the theory of molecular vibration and excitation (Hunt, 1977), it is possible to generate overtone vibrations when exposing a geological material to electromagnetic radiation. These overtones can be related to certain molecular groups, the hydroxyl (OH) group being the most common one capable of generating them. In quartz-based materials this typically relates to molecular water and metal-OH combinations (Hunt, 1977: 508). Overtones occur at frequencies that are multiples of the infrared vibration, and most of these end up in the near-infrared region (Osborne et al., 1993).

NIR analysis was conducted with an Analytical Spectral Device (ASD) LabSpec 4, using a contact probe (spot size: 10 mm). The ASD features a detection range of 350 nm – 2 500 nm, with spectral sampling of 1.4 nm in the visible and near-infrared range and 1.1 nm in the short-wave infrared range. Respectively, spectral resolution is 3 nm in the visible and near-infrared range, and 10 nm in the short-wave infrared range. Each object was measured against a white reference background and the collected measurements were averaged for each artefact. The data was restricted to the 1 000 nm - 2 500 nm range and mean-centred before Principal Component Analysis (PCA) modelling.

Raman

Raman spectroscopy shares similarities with NIRS in that they both can be used to infer molecular structures based on their vibrational properties within the near-infrared region (Nafie, 2001). By exposing a molecule to radiation with a monochromatic laser it is possible to induce a dipole moment in the molecule which generates the Raman effect. The subsequent light that is scattered contains both *Rayleigh* and *Raman scatter*, the former at a frequency of incident radiation and the latter at a shifted frequency (Dubessy et al., 2012). The spectrometer will measure the Raman scatter and generate a spectrum where the spectral line has shifted compared to the incident Rayleigh frequency. As the structure of a molecule will inform its vibrational mode, the point at which these shifts occur within the infrared region varies depending on the material (Smith and Carabatos-Nédelec, 2001).

The Raman instrumentation used was a portable i-Raman EX featuring a 1064 nm excitation laser (spot size: 85 μm). The spectral coverage of the instrumentation is 175 cm^{-1} – 2 500 cm^{-1} , with a resolution of 9.5 cm^{-1} . Integration time was set to 20 seconds with 30% power. After averaging the spectra for each artefact the results were baseline corrected in order to detrend the data. This was achieved using Lieber and Mahadevan-Jansens' (2003) algorithm for polynomial fitting, with the ChemoSpec package (Hanson, 2016). The spectra were then mean-centred before PCA.

X-Ray Fluorescence (XRF)

XRF spectroscopy is a well-established method for petrographic characterization in archaeology (Hall, 1960; Shackley, 2011a). In a non-destructive context, where the sample is not homogeneous, it is necessary to correct for matrix effects caused by the presence of other elements in a sample (Sitko and Zawisza, 2012: 143-159). Portable XRF instruments typically feature a set of filters to achieve this, calibrated for different mediums (e.g. soil, metals, minerals) (Knight et al., 2021: 2).

Measurements were collected using the Energy Dispersive (ED) Thermo Scientific Niton XL5 Analyzer (spot size: 8 mm), connected to a portable test stand. The reference calibration used for element quantification was mining mode (Knight et al., 2021: 2; Thermo Fisher Scientific, 2018). The integration time was set to 130 seconds. Higher spectral resolution can be achieved if used with a Wavelength Dispersive (WD) XRF system (Menne et al., 2020). However, these are limited to lab-based environments and not applicable in the field, which is central to the current study.

As the variables in XRF analysis are given as proportions of a constant sum (e.g. percentage, parts per million (ppm)), this creates something referred to as the *closed sum* effect (Pawlowsky-Glahn and Egozcue, 2006). This means that if one element was to change in value, others would follow to maintain the constant (Grunsky and Caritat, 2020). This has implications for classical statistical methods and is managed by transforming the data using log-ratio transformation (Aitchison, 1999). Currently there are three main methods; additive log-ratio (alr), centered log-ratio (clr) and isometric log-ratio (Pawlowsky-Glahn et al., 2015). In the PCA, the Principal Components are orthogonal and thus the relationships between variables treated with log-ratio transformation are

linear and independent of the total concentration (e.g. Reimann et al., 2012). With this transformation, PCA is thus suitable for exploring geochemical trends related to the rock-forming process without being impacted by the closed sum effect.

As the current dataset features values below the Limit of Detection (LOD) these were treated as NULL (or “missing values”) during PCA. A LOD value is defined as a measured value 3 times lower than the standard deviation for that measurement. Missing values are not permitted in the PCA and thus had to be imputed before the analysis, which was performed using the *lrEM* function from the *zCompositions* R package (Palarea-Albaladejo and Martin-Fernandez, 2015). *lrEM* stands for “Log-ratio Expectation-Maximisation”, which is an algorithm used to impute “left-censored data” (e.g. values below LOD, rounded zeros). Following log-transformation the data was mean-centred and scaled to unit variance before PCA. To prevent quantification errors related to samples size artefacts that were less than 10 mm in length or width were excluded from the model (Shackley, 2011b: 9; Lundblad et al., 2008).

Principal Component Analysis (PCA)

The data were evaluated using PCA, an unsupervised exploratory technique for reducing the dimensionality of a dataset (Geladi and Linderholm, 2020). Analysis was performed using the base R *prcomp()* function (R Core Team, 2021a, 2021b).

Results

Spectra and PCA loadings for each instrumentation can be found in the supplementary data. An open repository with the code used in the analysis is linked in the *Data availability* section.

Near Infrared Spectroscopy (NIRS)

NIRS is less effective on translucent material, such as a pure quartz crystal, as the absence of impurities in the material will result in little to no reflection/absorbance of light (Hunt, 1977). Similarly, it can be difficult to work with dark materials as most of the light produced by the instrument will be absorbed, with the high absorbance potentially obscuring visible features in the spectra. The dark material exhibits a wider range of absorbance, most likely due to the range of hues within the group, and generally shows less distinct peaks than the material with a lighter hue.

The spectra were evaluated using Savitzky-Golay (SG) filtering, a smoothing technique widely applied in spectroscopy (Chryssikos and Gates, 2017: 78-81). 2nd derivative SG can amplify weaker peaks in the spectra, although at the risk of amplifying noise (Mark and Workman, 2021: 351-397; Schmid et al., 2022). After reviewing the *dark* group using SG filtering, 45 out of a total of 93 artefacts were kept in the analysis.

Significant peaks were identified at 1 400 nm, 1 900 nm, 2 200 nm, and 2 350 nm. These features are all the result of overtones and vibration combinations of OH groups, with the two first peaks at 1 400 nm and 1 900 nm being indicative of molecular water (Fig. 4) (Hunt, 1977: 508-510; Sciuto et al., 2019). OH groups can produce a response in a number of different fields in the same material, with metal-OH combinations occurring in the 2 000 nm - 2 500 nm region. While there are exceptions, a more intense 2 200 nm band has typically been related to aluminium hydroxide (AlOH), and a more intense 2 350 nm band to magnesium hydroxide (MgOH) (Hunt, 1977: 509; Clark et al., 1990: 12664). In the current dataset the 2 200 nm band is typically the more intense band.

The 2 200 nm and 2 350 nm absorption bands can be found in mica, such as muscovite and biotite, which can be found in quartzite (Clark et al., 1990: 12; Hunt, 1977: 510; Ramanaidou et al., 2015: 207). Although muscovite and biotite share some band positions, the altered Al content as a response to metamorphism has been documented to shift some positions and increase others, such as the 2 250 nm band for biotite (Duke, 1994). As can be seen in the average spectra in **?@fig-nir-spectra-summary**, the dark material exhibits an additional peak at ~2 250 nm, which may indicate the presence of biotite and a different metamorphic grade.

Two smaller features were recorded, albeit vague and difficult to make out in the non-processed spectra, at 1 065 nm and 1 300 nm (**?@fig-nir-spectra-summary**). These could be caused by ferrous iron (Fe^{2+}) (Hunt, 1977: 503-504), which has been demonstrated to produce a response in the NIR in a number of minerals. In studies of olivine the absorption region has been determined to be broad and centred around 1 000 nm, but with three features at 900 nm, 1 100 nm and 1 300 nm (Trang et al., 2013). Alternatively, weak absorption features (OH) have also been noted in the 950 nm and 1 150 nm bands, particularly among clays. However, these overlap with the Fe^{2+} bands

in, for example, biotite (Adams, 1975: 104-106). It is possible that the features at 1 065 nm and 1 300 nm can be linked to the presence of ferrous iron, but it is difficult to say what the contributing mineral is at this stage.

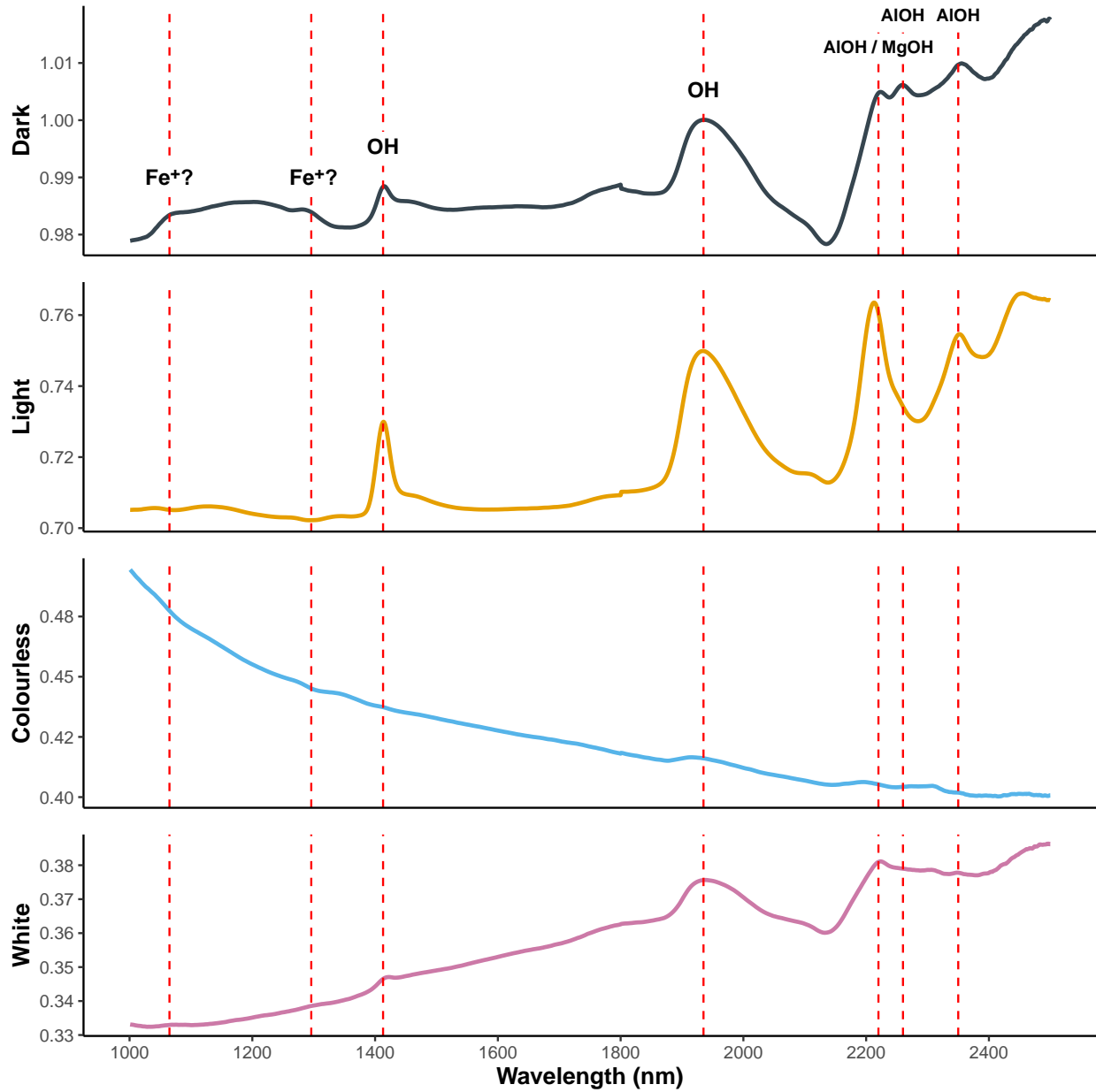


Fig. 4: The main features in the NIR spectra can be related to overtones and vibration combinations of OH groups. The 1 400 nm and 1 900 nm peaks are indicative of molecular water, and common in quartz-based materials. The 2 200 nm and 2 350 nm bands indicate metal-OH combinations, where a more intense 2 200 nm band has typically been related to the presence of AlOH, and a more intense 2 350 nm band MgOH. Although difficult to detect in the non-processed spectra, weaker features also appear at 1 065 nm and 1 300 nm, that may be the result of ferrous iron (Fe^{2+})

The loading lines for the PCA can be seen in the supplementary data. The first principal component (PC 1) shows a strong trend (98.71 %) that seems to largely correlate with the absorbance of the material (Fig. 5). This can be seen in the trend of darker material clustering towards the positive side of PC 1, with lighter towards the negative. A slight difference in the clustering of material with a light hue can also be seen along PC 2 (1.08 %). Objects with a white or light grey hue gravitate towards the bottom left of the score plot, while material that displays some translucence cluster towards the top left. There are objects that break this trend, however, such as sample 255 in the bottom right of Fig. 5 :A.

Whilst the explained variance of PC 3 is low, (0.13 %), it still contains a number of the aforementioned features visible in the spectra (inverse to PC 1). Adding PC 3 to a score plot (Fig. 5 :B), however, provides little new information apart from a couple of samples, mainly from the light group, that break away from the larger cluster.

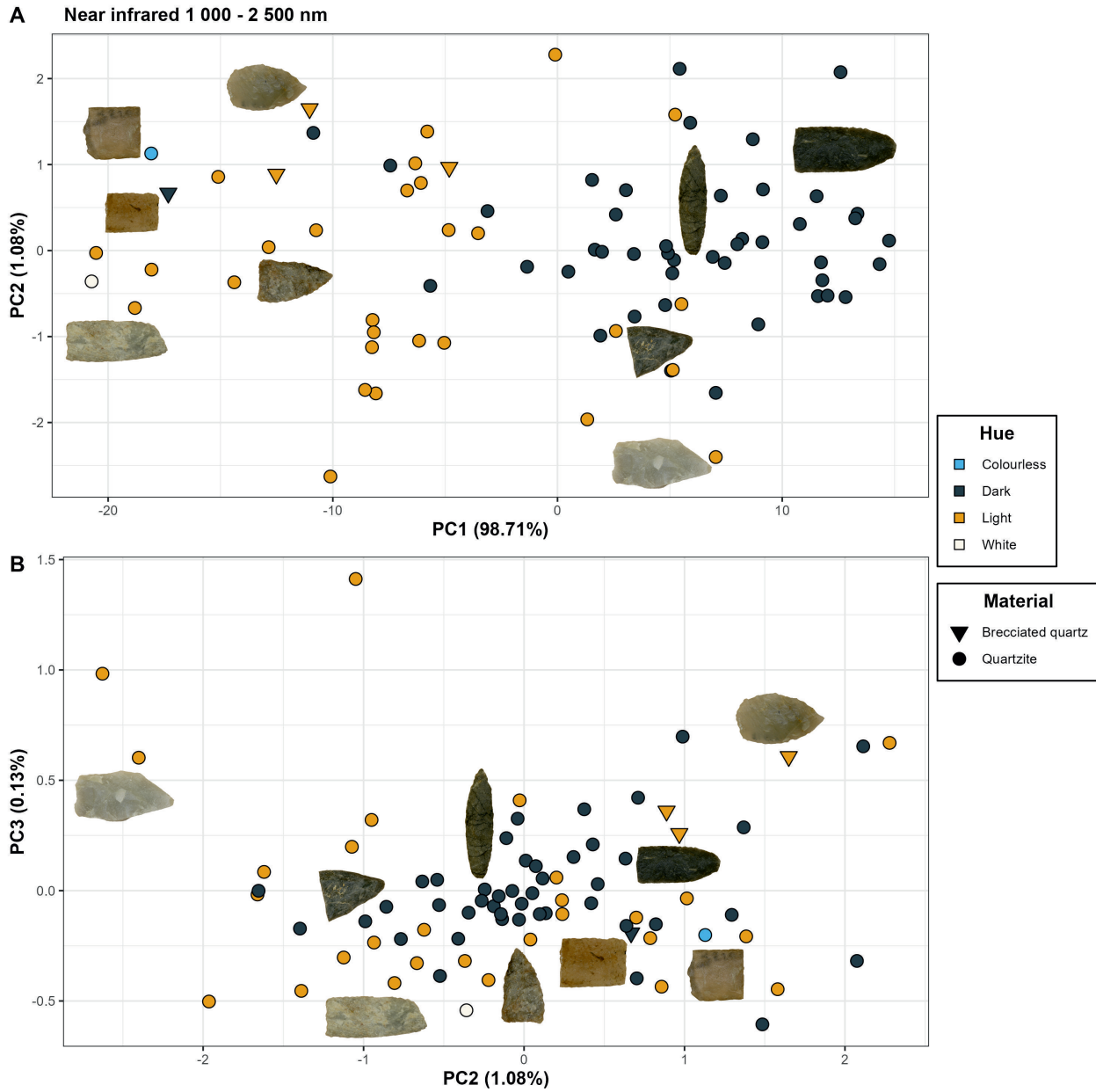


Fig. 5: NIR PCA score plot for PC 1-3: a) dark and light material is separated out along PC 1, due to absorbance, with white and colourless material separating along PC 2, b) PC 3 adds little new information, mainly separating three of the light samples

Raman

There are two distinguishing features present in the Raman data (Fig. 6)), one which can be related to quartz and another that may indicate the presence of carbon (C) structures. The three initial

bands at $\sim 128\text{ cm}^{-1}$, $\sim 200\text{ cm}^{-1}$ and $\sim 460\text{ cm}^{-1}$, are some of the more intense quartz bands (Zhong et al., 2021), with the strongest peak occurring at 460 cm^{-1} (Gillet et al., 1990).

second feature shows as two peaks at around $1\,287\text{ cm}^{-1}$ and $1\,598\text{ cm}^{-1}$, and dominates the spectra in terms of intensity for the darker samples. These positions fall within what is referred to as the *D* and *G* band respectively, and have been observed in spectroscopic studies of graphite (Cesare and Maineri, 1999). The *D* band occurs as a result of disordered C structures, whilst the *G* band is indicative of sp^2 C networks and caused by stretching in the C bonds, which is common in graphite-based materials (Cohen-Ofri et al., 2006; Lee et al., 2021; Vollebregt et al., 2012). The *G* band peak falls within the expected position, whereas the position of the *D* band is more commonly identified as being in the $1\,330 - 1\,350\text{ cm}^{-1}$ region. It has, however, been documented that the dispersive behaviour of the *D* band can cause a frequency change as a result of the energy of the incident laser (Pimenta et al., 2007: 1280). This could thus explain the discrepancy between the observed peak in the dataset and the literature.

In addition to the more intense features described above, a number of weaker peaks can also be seen in the spectra. Some of these could be additional quartz bands (Zhong et al., 2021), such as a weak peak at 1160 cm^{-1} that is somewhat obscured by the *D* band. Two peaks can also be found in the $700 - 800\text{ cm}^{-1}$ band range. The 700 cm^{-1} band has been identified as one of the aforementioned quartz bands. Studies of clay minerals (Kloprogge, 2017), and iron ore minerals (Ramanaidou et al., 2015), have also generated a response related to Si, Al and OH vibrations within the $700 - 800\text{ cm}^{-1}$ region.

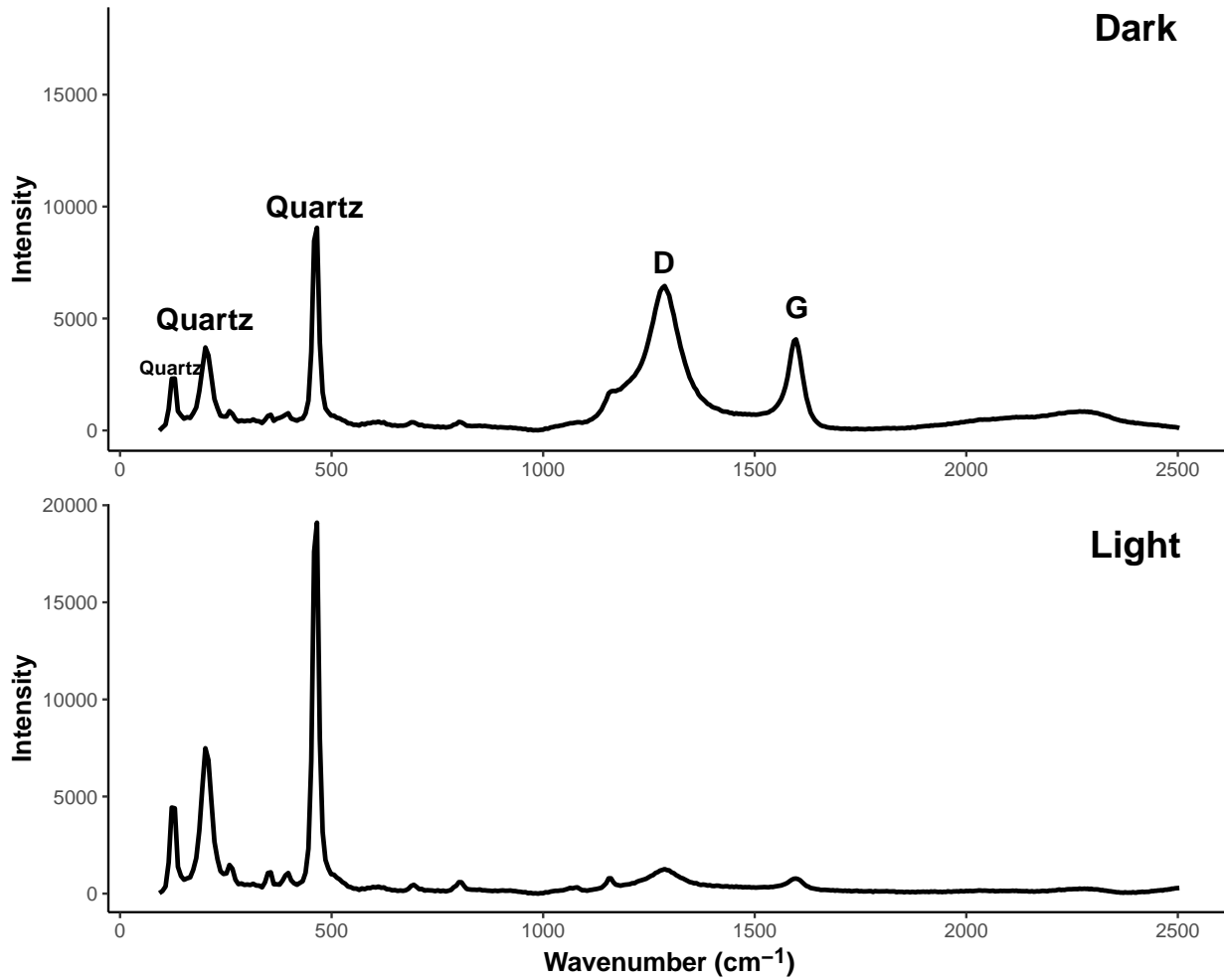


Fig. 6: Averaged and baseline corrected Raman spectra for the light and dark groups. The features can be related to quartz and carbon structures in the material. The initial three peaks in the $100 - 500 \text{ cm}^{-1}$ range correspond to some of the more well-known vibration modes of quartz. The 1287 cm^{-1} and 1598 cm^{-1} peaks fall within what is referred to as the D and G band respectively, indicating the presence of carbon structures. The white and colourless spectra only show significant peaks for quartz (see Supplementary Data).

The PCA model (Fig. 7) shows a clear trend along PC 1 (75.9 %) related to the quartz and D/G peaks. Samples where the D/G peaks dominate in terms of intensity cluster towards the positive side of PC 1, with those that completely lack or have weaker D/G bands on the opposite side. Similarly, along PC 2 (21.2 %) the samples that have higher intensity D/G peaks gravitate towards the top of the score plot. Worth noting are two dark samples that completely lack D/G peaks, placing them among the light material in the left side of the plot. One of these is a *brecciated quartz* sample with a dark yellow tint, and thus more a sign of the difficulties with assigning a generic hue to the material. The second sample, however, stands out from the rest of the material. It is a point preform made from a grey material with a rough texture, and possible layering, with larger quartz

crystals. It does not fit with the “expected” image of a quartzite and may be a case of erroneous archaeological classification. The addition of PC 3 (2.1 %) provides no new information, but rather separates out those samples with a higher level of noise.

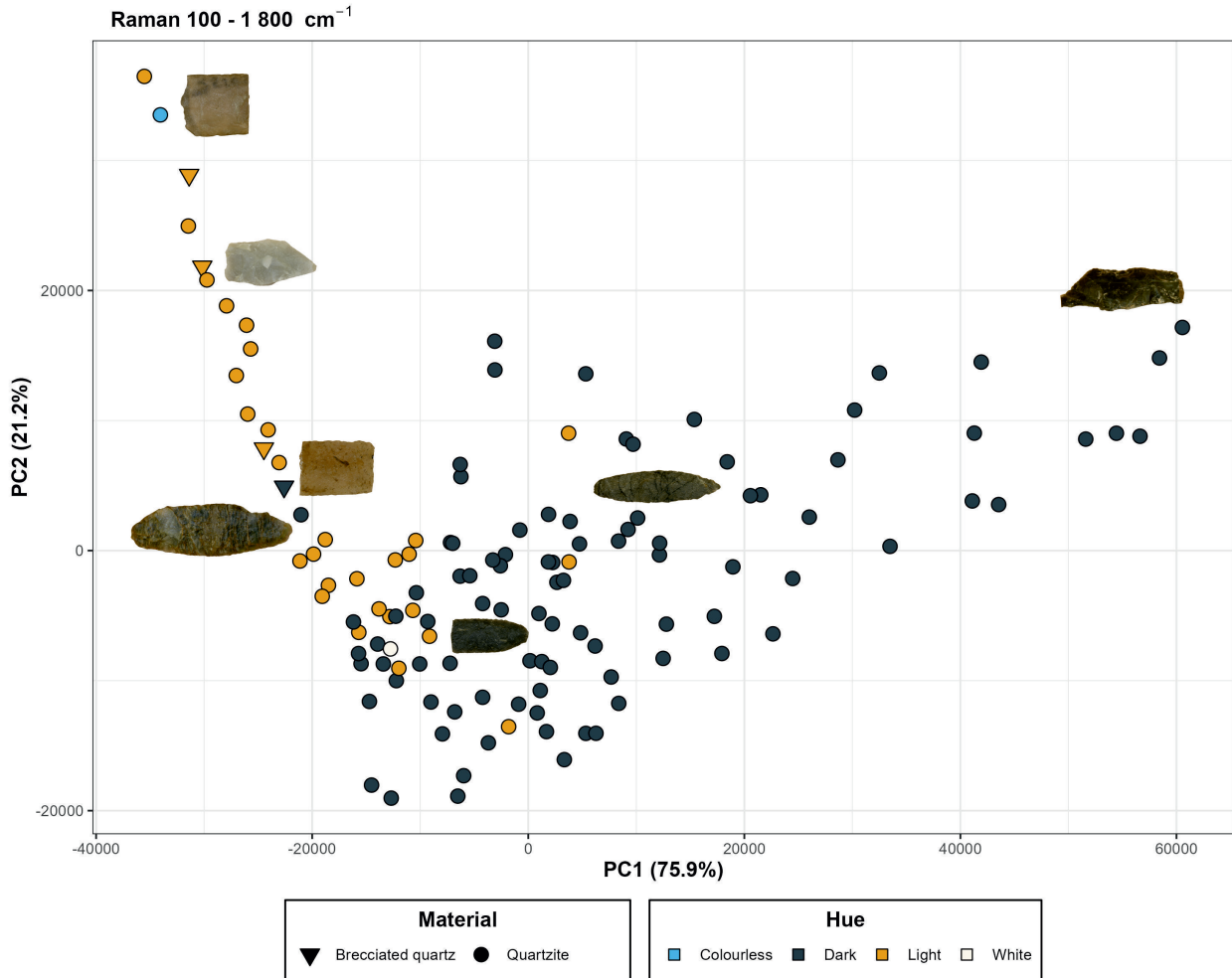


Fig. 7: PCA score plot for Raman data. Objects that feature only quartz peaks are clustered towards the top left of the plot, whilst the darker material that feature dominant D/G peaks are distributed towards the right of the plot. In the middle cluster the samples feature both quartz and D/G peaks, with those that have higher intensity D/G peaks in the bottom of the cluster.

X-Ray Fluorescence (XRF)

The XRF spectrometer is not capable of detecting all the common elements, and the software therefore calculates a balance (BAL) that represents the remaining unquantifiable elements in a sample. The elements represented in this group are all those with an atomic number lower than $_{12}\text{Mg}$ (Thermo Fisher Scientific, 2018). The analysis shows that $_{14}\text{Si}$ makes up the main bulk of the material, with $_{13}\text{Al}$ recorded up to $\sim 5\%$ for some samples (Fig. 8). The majority of the readings resulted in $_{14}\text{Si}$ content of less than 50%, as well as a BAL between 40 – 70%, meaning that a significant portion of the material remains unknown. Whilst this could be due to the limitations of the instrumentation, it could also be a result of the sampling. As quartzite is a metamorphic rock where the distribution of quartz is not necessarily uniform in the material, the sample point can have a considerable influence on the measurement. Out of a total of 126 samples 28 measured a $_{14}\text{Si}$ content higher than 90%. Certain elements recorded a high number of values below the LOD (“missing values”), including $_{12}\text{Mg}$, vanadium ($_{23}\text{V}$), manganese ($_{25}\text{Mn}$), yttrium ($_{39}\text{Y}$) and zinc ($_{30}\text{Zn}$). Although in the case of $_{12}\text{Mg}$ and $_{25}\text{Mn}$ the recorded values reached up to 0.3% and 3% respectively.

Initial analysis used clr transformed data, but encountered issues related to the structure of the $_{14}\text{Si}$ values. Instead log10-transformation was used, producing a similar model, but one that managed the loading for $_{14}\text{Si}$ better. The PCA was run twice, firstly with the $> 90\%$ $_{14}\text{Si}$ samples included and secondly excluded. The initial PCA (model A), with the full dataset included, resulted in 3 PCs with an eigenvalue above 1, and a cumulative explained variance of 66.15%. K-means cluster analysis was performed on the PCA data in order identify potential groups with similar elemental composition. Using the elbow graph method 3 clusters were deemed suitable for the analysis.

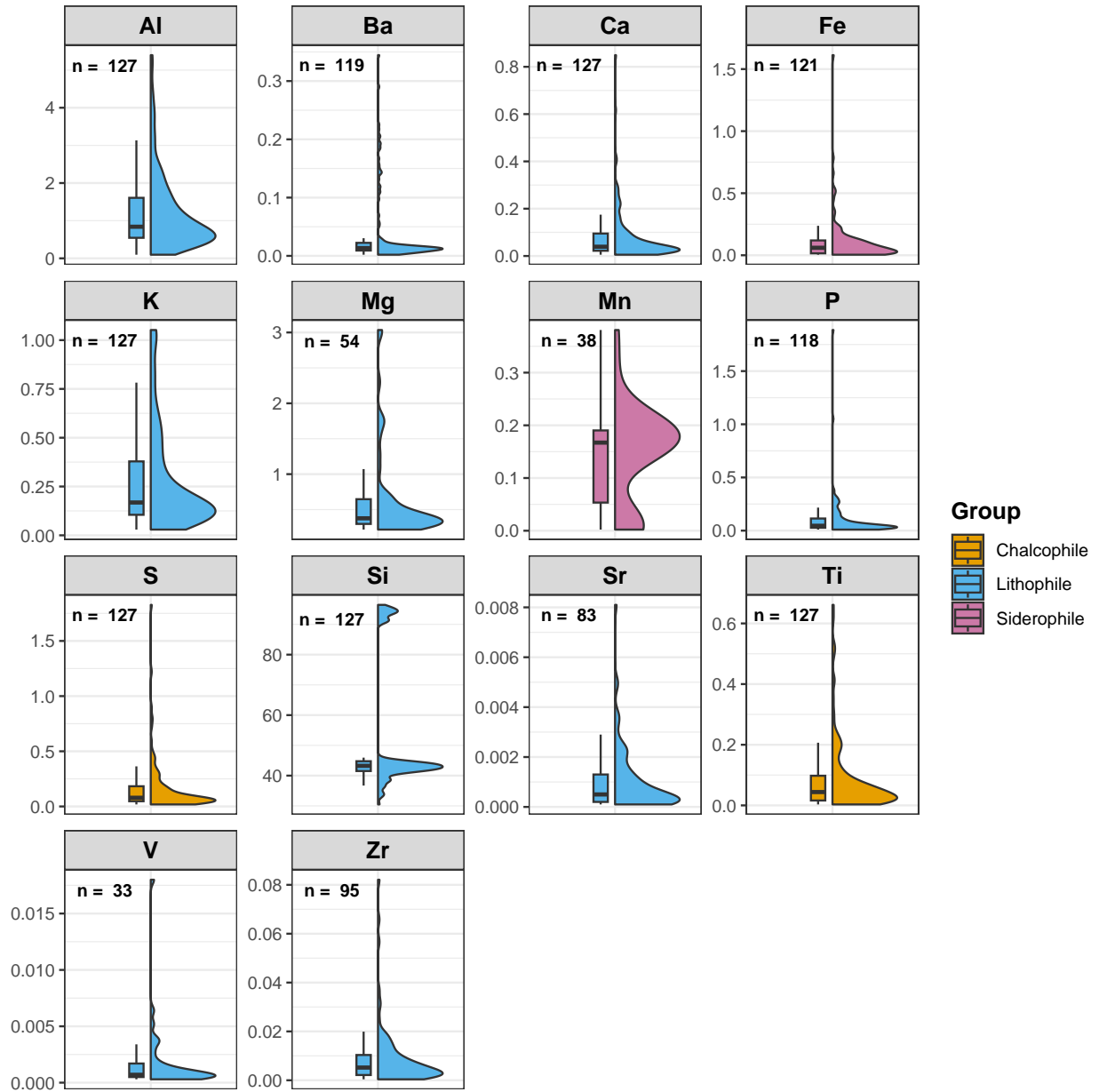


Fig. 8: Violin plots of the XRF values per element. Median and interquartile range is represented with a boxplot, with the half-violin showing kernel density estimation. Number of values above LOD is noted by n. Of particular note is the bimodal distribution of Si values. Y and Zn were left out as they had less than 30 values above LOD.

As can be seen in the score plot (Fig. 9 :A), the three K-means clusters remain separated. Cluster 1 is made up of those samples that feature a high ^{14}Si content ($> 90\%$). There is no real pattern to this cluster aside from higher ^{14}Si values with lower iron (^{26}Fe) and zirconium (^{40}Zr) values. Loadings for elements expected to follow changes in ^{14}Si content also end up near cluster 1 (e.g. Al, calcium

(Ca)).

Cluster 2 is distinguished by a higher titanium ($_{22}\text{Ti}$), $_{26}\text{Fe}$ and $_{40}\text{Zr}$ content. It mainly features samples with a dark hue, with the few samples from the light group being grey in colour and arguably somewhere in between a “dark” or “light” hue. $_{13}\text{Al}$ and potassium ($_{19}\text{K}$) is similarly higher in cluster 2 than cluster 3, which is in turn marked by its, on average, lower elemental content than the other two clusters. As $_{13}\text{Al}$ and $_{19}\text{K}$ are indicative of a sedimentary depositional context that has been subject to metamorphism (Hazen and Morrison, 2022), and the cluster with higher values may thus indicate samples with a different grade of metamorphism. Cluster 3 features a more limited range of values between the samples and includes all the *brecciated quartz*.

In the second PCA model (model B) four PCs feature an eigenvalue above 1 with a cumulative explained variance of 71.51%. Three clusters were deemed suitable for the K-means analysis (Fig. 10). The range of values is more limited in cluster 3, with overall lower values than compared to the other clusters (Fig. 9 :B). The *brecciated quartz* samples all remain in cluster 3, along with mainly light-to-colourless samples. Cluster 2 features the main bulk of darker samples with higher $_{22}\text{Ti}$, $_{26}\text{Fe}$ and $_{40}\text{Zr}$ values. Cluster 1 likewise feature a large portion of the darker materials, with comparable $_{22}\text{Ti}$, $_{26}\text{Fe}$ and $_{40}\text{Zr}$ values. It also has higher values of $_{12}\text{Mg}$, $_{13}\text{Al}$, $_{16}\text{S}$, $_{19}\text{K}$, and $_{20}\text{Ca}$.

$_{38}\text{Sr}$ was detected at trace amounts. It is a lithophile element that can substitute for $_{20}\text{Ca}$ in sulphates, feldspars, mica and clays (Ahijado et al., 2005; Banner, 1995), which might be one explanation for its presence in cluster 1 in model B. Nearly all samples with $_{38}\text{Sr}$ are located in cluster 2 in model A.

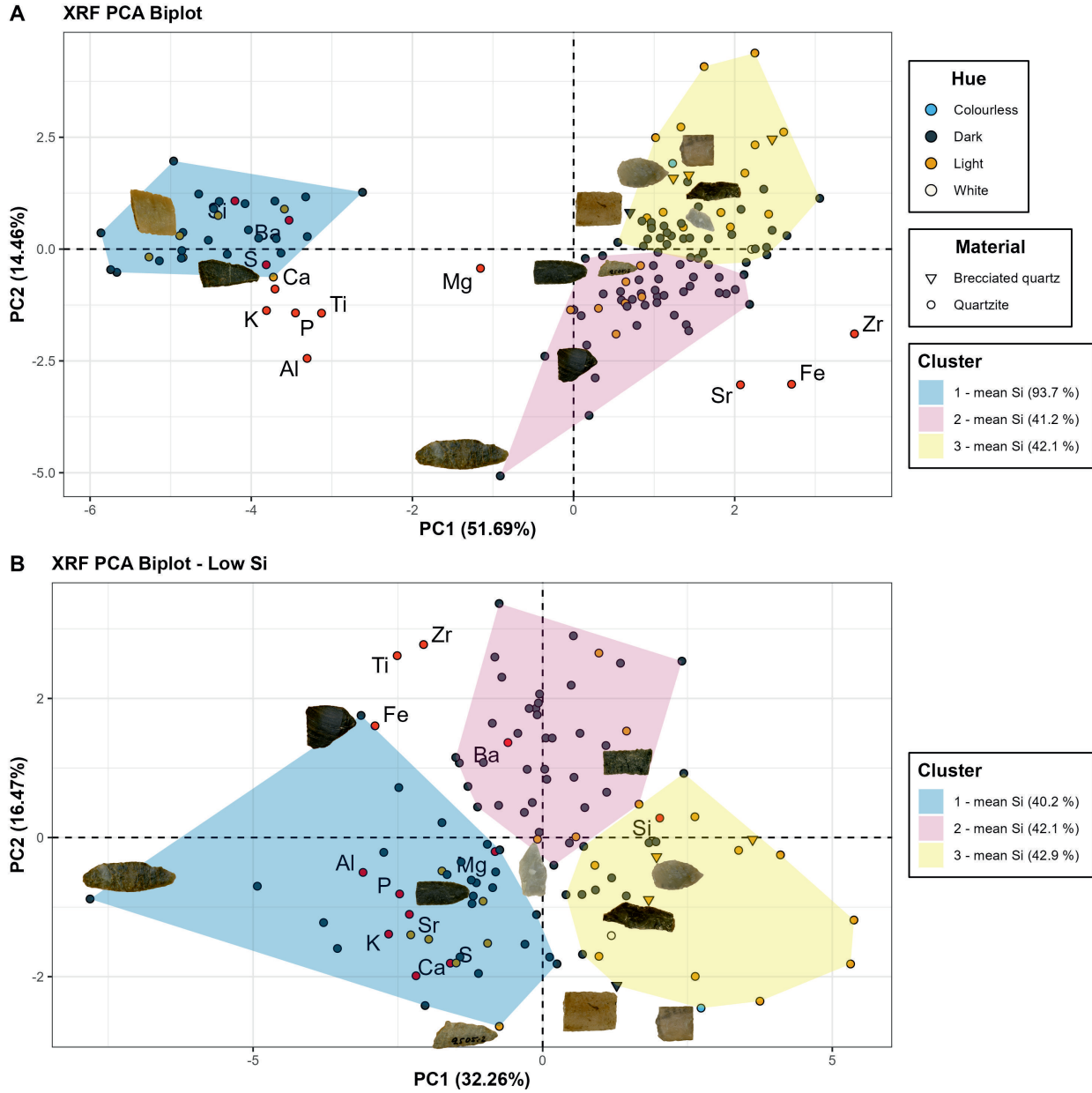


Fig. 9: XRF PCA score plots: a) Score plot featuring the full dataset, cluster 1 includes all samples with $\text{Si} > 90\%$, while the remaining samples seem to cluster based on Fe and Zr content. This results in most of the darker materials clustering towards the bottom of the plot. b) Score plot with $> 90\%$ Si samples excluded. Similar to plot A there is a separation based on Fe and Zr values, with darker material towards the bottom of the plot. Light-to-colourless samples remain largely together in cluster 3. Cluster 1 stands out by featuring slightly lower Si, Fe, Ti, and Zr values, but higher values in Al, Ca, K, and Mg

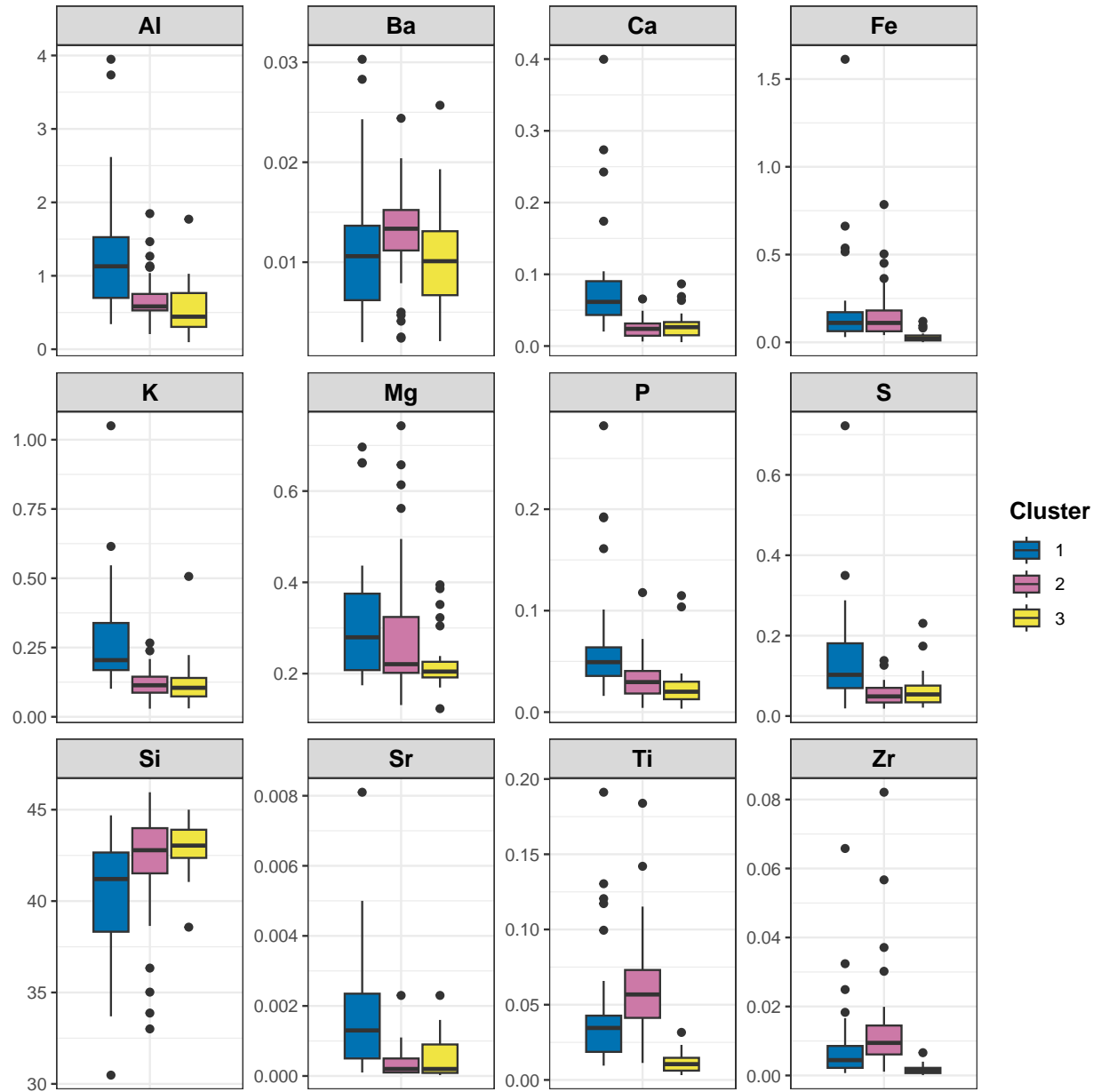


Fig. 10: Boxplot of XRF values (%) in PCA model B, grouped by K-means cluster. Cluster 1 is made up of samples with lower values of Si, but higher values for those elements that are typically associated with Si (e.g. Al, Ca). Cluster 2 includes the samples with higher Fe/Ti/Zr content, whilst cluster 3 is mainly distinguished by a higher Si content and low Fe/Ti/Zr content

The K-means cluster analysis of model B is visualised in the NIRS PCA score plot, which further emphasizes the variation within the general colour groups (Fig. 11). Cluster 2, with higher $_{26}\text{Fe}$ and $_{40}\text{Zr}$ values, mainly coincides with the darker material to the right side of the plot. This was

expected as the trend along PC 1 in the NIR PCA mainly separates the material according to absorbance. Cluster 3 in turn coincides with the lighter material in the opposite side of the model. Cluster 1, however, is fairly evenly distributed within the model along PC 1 and PC 2.

The variation that occurs within the general colour groups can be further exemplified by looking closer at three samples selected from the dark group, that each belong to a different K-means cluster. They all share a similar hue with D/G peaks detected in the Raman analysis (Fig. 12). All three samples have similar absorbance values, but sample 391 exhibits differences in the spectra when compared to the other two samples. Samples 386 and 404, however, are separated primarily in the XRF analysis.

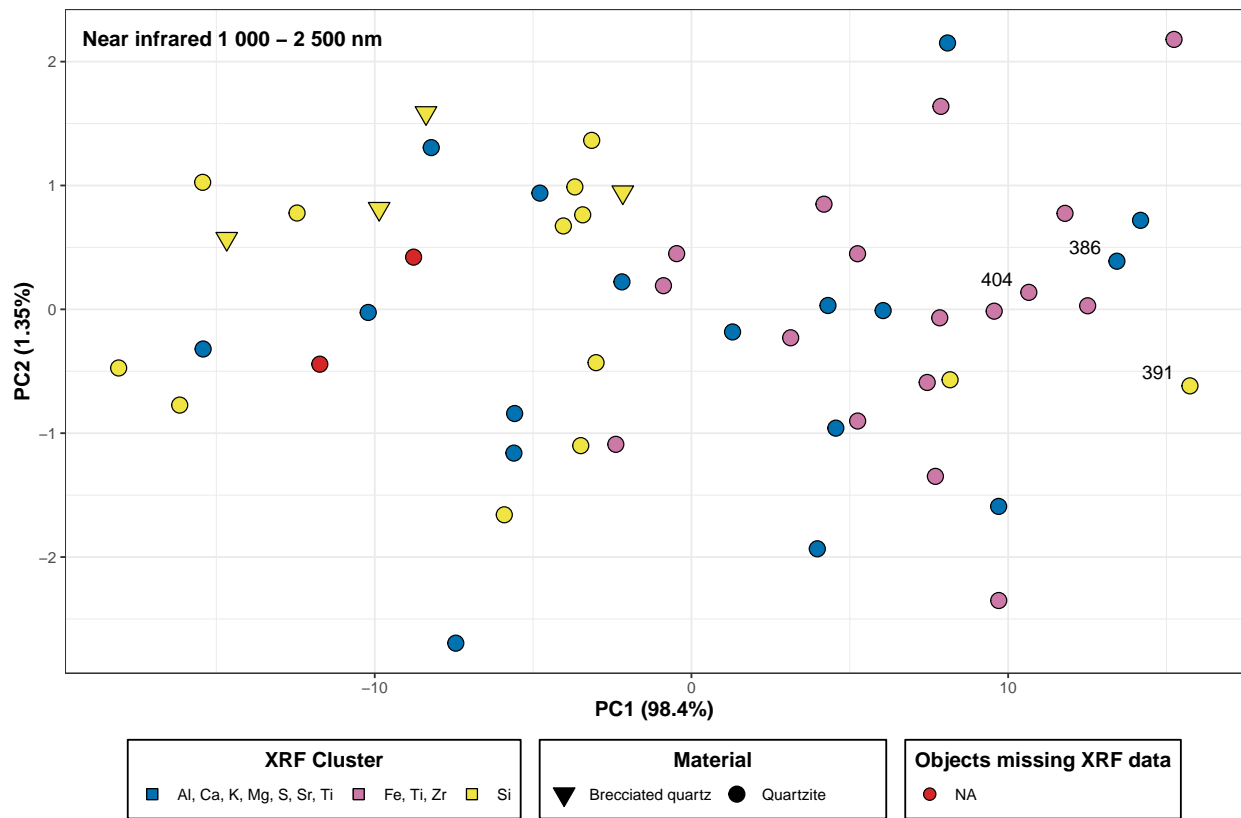


Fig. 11: NIR PCA score plot for PC 1-2, with the K-means cluster from XRF PCA model B visualised in the colour of the points. Red points are samples that were excluded in the XRF PCA. The trend separating dark-light samples in the NIR PCA mostly keeps cluster 2-3 separated, showing some overlap in the results, but cluster 1 is fairly evenly distributed in the score plot. This means that whatever differences can be discerned in the compositional data does not seem to be detectable using the ASD.

Sample	Mg(%)	Al(%)	Si(%)	P(%)	S(%)	K(%)	Ca(%)	Ti(%)	Fe(%)	Sr(%)	Zr(%)	Ba(%)
386	0.2568	0.7762	38.8005	0.0515	0.1529	0.1703	0.0636	0.0656	0.5157	0.0001	0.0096	0.0049
391		0.3044	43.0357	0.0367	0.2306	0.1200	0.0636	0.0105	0.1195	0.0003	0.0012	0.0067
404		0.7130	41.5187	0.0263	0.1263	0.1447	0.0442	0.1420	0.3636	0.0005	0.0102	0.0120

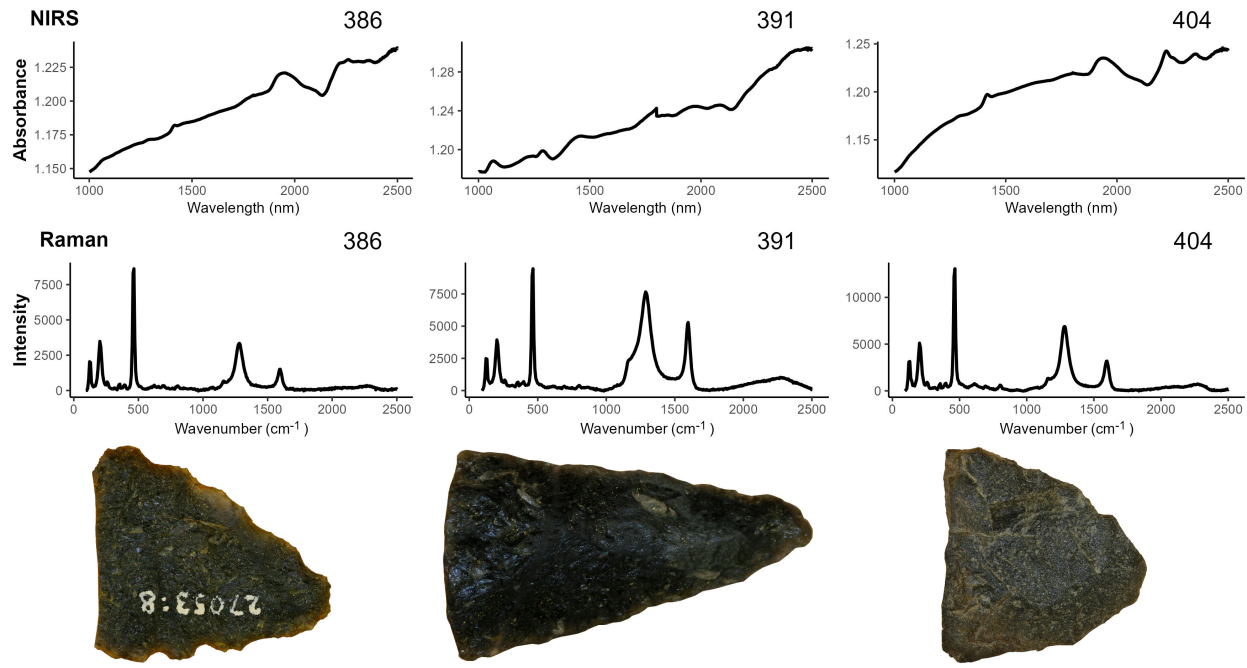


Fig. 12: Comparison of three dark samples from separate K-cluster groups (model B). Sample 391 from cluster 3 stands out the most with visible differences in both the NIR and Raman spectra, when compared to the other samples.

Discussion

A screening-based approach to material analysis using non-destructive spectroscopy is particularly useful in regions with complex geology, such as Northern Sweden, where little development has been made in the chemical characterization of quartzite. With so many unknowns, it is better to first assess the variability within the material before engaging in more detailed and targeted analysis. Non-destructive methods are capable of generating large and expansive datasets with relative ease, and little risk to the material in question. When coupled with exploratory data analysis, these techniques are a useful starting point for an empirically grounded description of a material and for identifying any features of note. Where feasible, the material can then be further analysed

with destructive methods capable of providing a higher resolution view of chemical and physical characteristic, potentially leading to its general characterisation (e.g. Blomme et al., 2012; Prieto et al., 2020; Prieto et al., 2019).

The results presented here have increased the state of knowledge of the chemical and structural variation that exists under the umbrella of what archaeologists refer to as quartzite within the Västerbotten area. These results are applicable to neighbouring regions and beyond, and should help in furthering research into prehistoric tools in Scandinavia and other regions. The material exhibits considerable variation in terms of texture and colour, and the results suggest that the initial classification, based on the archaeological documentation, may have included mistakes. These mistakes, whilst of little consequence for site interpretation individually, may introduce considerable noise, or “messiness”, when aggregating data for large scale spatio-temporal analyses (Gattiglia, 2015: 2). The results also highlight some of the implications that the choice of spectroscopic analysis method may have for the identification of features in a material. In particular, they demonstrate that reliance on any individual method may introduce limitations which could make material classification difficult or misleading.

The strength of this study is in the multispectral approach; the data generated from each method providing a complementary image of the structural and compositional nature of the material. Although Raman spectroscopy generated a limited amount of information in comparison with the other methods, the graphite structures identified in the material will likely be significant in future provenance studies. The utility of Raman spectroscopy as a screening tool, and in comparison to NIRS and XRF, seems to be somewhat limited when applied to quartz-based materials. Similarly, the broad bands in NIRS spectra are complex and can be difficult to interpret. Nevertheless, insights from the metal-OH bands suggest that more information on metamorphic grades may be obtainable. If the bands are related to the Al content of the material and the presence of mica, then the band positions may indicate differing metamorphic grades in the material (muscovite - biotite). This will need to be evaluated in more detail in future studies.

Whilst NIRS and Raman may be somewhat limited in the characterization of quartz and quartzite they have considerable potential when combined with the XRF. The complementary information about the structural elements in the material can help guide interpretation of the compositional data. Ideally these different sources would be fused using methods such as multi-block PCA to better assess key variables contributing to the model (Mishra et al., 2021).

The metamorphic nature of quartzite presents a particular challenge for spectroscopic sampling. The material frequently exhibits mineral inclusions that produce a varied surface, and the spot size of the probe will affect the user's ability to capture a representative area of the artefact. Likewise, the artefact's shape, type, and preservation significantly influence the availability of surfaces suitable for sampling. This can be further compounded by certain limitations with the technique itself. Both NIRS and Raman can be affected by saturation on darker materials, due in part to the absorbance, obscuring spectral features. Although some of these issues may be overcome with other non-destructive methods, such as Hyperspectral Imaging (Sciuto et al., 2019), the arguably more affordable techniques presented here produce valuable data. Not everyone will have the benefit of working with all three instrumentations however, and in such situations XRF seems to provide more utility. Although WD-XRF systems will provide higher spectral resolution and element detection (Menne et al., 2020), portable ED-XRF has come a long way since its introduction, and instruments becoming commonly available in archaeological laboratories.

The spectroscopic features identified in this study relate to the diagenetic/paragenetic environment and are thus useful for locating potential geological sources in future field surveys. As quartzite is a metamorphic rock, there are two factors affecting its chemical and structural properties; the composition of the materials in the original depositional context, and the grade of metamorphism (in the case of sedimentary orthoquartzite it is mainly the former). The D/G bands indicating graphite in the Raman results imply that the material formed in carbon-rich formations. Alum shales and similar carbon-rich tectonic strata are present within the Scandian mountain chain (Stephens and Bergman Weiherd, 2020: 482-599), and it would be reasonable to expect C structures in quartzite or quartzite-like materials in the region. However, the term “graphitic quartzite” is seldom encountered in contemporary Swedish geological publications. Usage of the term can be found in an early 20th century description of an excursion to Storfjället, Tärna parish, by the Geological Society (Geologiska Föreningen i Stockholm, 1925). The occurrence of metamorphic rocks containing graphite, including schist and quartzite, in other regions (e.g. Gawęda and Cebulak, 1999; Ukar and Cloos, 2016) suggests that further studies of this material would be useful for provenance studies in Sweden.

The high representation of quartz and quartzite in the Mesolithic - Bronze Age lithic assemblages of Northern Sweden necessitates the development of methods for the characterization of these materials. They represent a primary lithic resource, and thus hold a critical position for understanding resource procurement, trade and exchange, and human mobility within the region (as well as other regions (e.g. Prieto et al., 2019). Whilst spectroscopic methods can provide new data for advancing the understanding of patterns in resource procurement in geologically complex areas, procurement is only part of the picture for resource management strategies during the Mesolithic – Bronze Age. These data can, however, be used to test the different scenarios which existing models represent (Bergman, 1995; e.g. Forsberg, 1985; Lundberg, 1997). For example, a transhumant settlement system in which inland groups, organised along the river valleys, utilize raw materials collected in the mountains, should leave evidence of material flow from the mountains to the forest inland. With high quality spectroscopic data from existing quartzite artefacts, a predictive model could be built to forecast the type of material expected at other sites. Multiple hypotheses and models could then be tested, and revised, on the basis of further data from new archaeological excavations and geological exploration. The uncertainty of the detailed geology of the region, and the potential noise that glacial disturbance will have introduced, would require that multiple scenarios are tested. A more robust geological resource model could be developed by fusing data from multiple types of spectroscopic instrumentation [e.g. multiblock PCA; Mishra et al. (2021)].

Conclusion

This study provides, through a non-destructive multispectral approach, empirical insights into the variability of quartzite material in Northern Sweden. The development of non-destructive screening methods provides a good initial basis for future detailed studies of quartz and quartzite material. This is especially valuable in geologically complex regions where there is an absence of reference

materials and ambiguous distribution of potential geological sources. Through the use of multiple instrumentations, the study has identified a number of features in quartzite that may be relevant to its future characterization. These include different forms of mica (NIRS), graphite (Raman), and iron content (ED-XRF). When coupled with exploratory data analysis, and with the addition of further geological and archaeological data, it should be possible to generate hypotheses on the flow of these materials in the Mesolithic – Bronze Age of the region. These hypotheses could then be tested through the analysis of material from new excavations and surveys. Targeted studies using destructive methods (e.g. thin sections analysis, laser ablation), capable of providing more detailed analysis and potentially a classification of the material, could be strategically employed to increase the robustness of the study. In order to truly advance the topic of prehistoric raw material management in Northern Sweden, it will be necessary to combine such studies with both archaeological and geological models. These will need to integrate archaeological and geological survey data with theories of resource procurement and economic strategies, ice sheet and glacial flow dynamics and detailed Quaternary geological mapping.

Acknowledgements

We would like to thank Västerbottens museum (www.vbm.se) for access to their collections, and Susanne Sundström in particular for her assistance with preparing the artefacts. We would also like to acknowledge cooperation with the division of Biomass Technology and Chemistry at the Swedish University of Agricultural Sciences.

Author Contributions

Mattias Sjölander: Conceptualization, Data curation, Formal analysis, Methodology, Project administration, Resources, Software, Visualization, Validation, Writing - original draft, Writing - Review & Editing.

Johan Linderholm: Conceptualization, Methodology, Supervision

Paul Geladi: Formal analysis, Methodology

Philip I. Buckland: Writing – original draft, Writing - Review & Editing.

Statements and Declarations

Competing interests

The authors declare no competing interests.

Funding source

This work was supported by PhD funding and facilities at the Environmental Archaeology Laboratory at Umeå University.

Data availability

The code and data used to perform the analysis is openly accessible in an online repository at <https://doi.org/10.17605/OSF.IO/F6H98>.

References

- Adams, J.B., 1975. 4 - INTERPRETATION OF VISIBLE AND NEAR-INFRARED DIFFUSE REFLECTANCE SPECTRA OF PYROXENES AND OTHER ROCK-FORMING MINERALS, in: KARR, C. (Ed.), Infrared and Raman Spectroscopy of Lunar and Terrestrial Minerals. Academic Press, pp. 91–116. <https://doi.org/10.1016/B978-0-12-399950-4.50009-4>
- Ahijado, A., Casillas, R., Nagy, G., Fernández, C., 2005. Sr-rich minerals in a carbonatite skarn, Fuerteventura, Canary Islands (Spain). *MINER PETROL* 84, 107–127. <https://doi.org/10.1007/s00710-005-0074-8>
- Åhman, E., 1967. Riksantikvarieämbetets norrlandsundersökningar 4. Petrografisk översikt av Umeälvs materialet. *Fornvännen* 8–11.
- Aitchison, J., 1999. Logratios and Natural Laws in Compositional Data Analysis. *Mathematical Geology* 31, 563–580. <https://doi.org/10.1023/A:1007568008032>
- Banner, Jay.L., 1995. Application of the trace element and isotope geochemistry of strontium to studies of carbonate diagenesis. *SEDIMENTOLOGY* 42, 805–824. <https://doi.org/10.1111/j.1365-3091.1995.tb00410.x>
- Bargel, T.H., 2003. Quaternary geological Mapping of Fennoscandia and Nordland: Deglaciation, Deposits, Stratigraphy, and Applications. Fakultet for ingeniørvitenskap og teknologi. Norges teknisk-naturvitenskapelige universitet, Fakultet for ingeniørvitenskap og teknologi.
- Baudou, E., 1992. Norrlands forntid : Ett historiskt perspektiv. Wiken, Höganäs.
- Baudou, E., 1978. Kronologi och kulturutveckling i mellersta Norrland under stenåldern och bronsåldern, in: Huggert, A. (Ed.), Studier i Norrländsk Forntid, Skrifter i Västerbottnisk Kulturhistoria. Västerbottens museum, Umeå.
- Bergman, I., 1995. Från döudden till varghalsen : En studie av kontinuitet och förändring inom ett fångstsamhälle i övre norrlands inland, 5200 f.kr. - 400 e.kr. Dept. of Archaeology [Institutionen för arkeologi], Umeå University, Umeå.
- Binford, L.R., 1979. *Organization and Formation Processes: Looking at Curated Technologies*. Journal of Anthropological Research 35, 255–273.
- Biörnstad, M., 1968. Forskningsprojektet Norrlands tidiga bebyggelse. *Fornvännen* 178–185.
- Blomme, A., Degryse, P., Van Peer, P., Elsen, J., 2012. The characterization of sedimentary quartzite artefacts from Mesolithic sites, Belgium. *Geologica Belgica* 15, 193–199.
- Broadbent, N., 1979. Coastal resources and settlement stability : A critical study of a Mesolithic site complex in northern Sweden. Institutionen för arkeologi, särskilt nordeuropeisk, Uppsala.
- Callahan, E., Forsberg, L., Knutsson, K., Lindgren, C., 1992. Frakturbilder.: Kulturhistoriska kommentarer till kvarts säregna sönderfall vid bearbetning. *Tor* 25, 27–63.
- Cesare, B., Mainieri, C., 1999. Fluid-present anatexis of metapelites at El Joyazo (SE Spain): Constraints from Raman spectroscopy of graphite. Contributions to mineralogy and petrology 135, 41–52. <https://doi.org/10.1007/s004100050496>
- Chryssikos, G.D., Gates, W.P., 2017. Chapter 4 - spectral manipulation and introduction to multivariate analysis, in: Gates, W.P., Kloprogge, J.T., Madejová, J., Bergaya, F. (Eds.), *Infrared and Raman Spectroscopies of Clay Minerals, Developments in Clay Science*. Elsevier, pp. 64–106. <https://doi.org/10.1016/B978-0-08-100355-8.00004-7>
- Clark, R., King, T., Klejwa, M., Swayze, G., Vergo, N., 1990. High spectral resolution reflectance spectroscopy of minerals. *Journal of Geophysical Research* 95, 12653–12680.
- Cohen-Ofri, I., Weiner, L., Boaretto, E., Mintz, G., Weiner, S., 2006. Modern and fossil charcoal: Aspects of structure and diagenesis. *Journal of Archaeological Science* 33, 428–439. <https://doi.org/10.1016/j.jas.2005.08.008>

- Dalpra, C.L., Pitblado, B.L., 2016. Discriminating Quartzite Sources Petrographically in the Upper Gunnison Basin, Colorado: Implications for Paleoamerican Lithic-Procurement Studies. *PaleoAmerica* 2, 22–31. <https://doi.org/10.1080/20555563.2015.1137684>
- Dubessy, Jean., Caumon, M.-C., Rull, F. (Eds.), 2012. Applications of Raman spectroscopy to earth sciences and cultural heritage, European Mineralogical Union notes in mineralogy. European Mineralogical Union and Mineralogical Society of Great Britain & Ireland, London.
- Duke, E.F., 1994. Near infrared spectra of muscovite, Tschermak substitution, and metamorphic reaction progress; implications for remote sensing. *GEOLOGY* 22, 621–624. [https://doi.org/10.1130/0091-7613\(1994\)022%3C0621:NISOMT%3E2.3.CO;2](https://doi.org/10.1130/0091-7613(1994)022%3C0621:NISOMT%3E2.3.CO;2)
- Forsberg, L., 2012. Asymmetric twins? Some reflections on coastal and inland societies in the Bothnian area during the Epineolithic and Early Metal Age, in: N., Wrigglesworth, A.&.M. (Eds.), Local Societies in Bronze Age Northern Europe. Equinox, London, pp. 31–55.
- Forsberg, L., 1989. Ett försök att urskilja sociala territorier i Norrland under bronsålder och förromersk järnålder. Regionale forhold i nordisk bronzealder: 5. Nordiske symposium for bronzealderforskning på Sandbjerg Slot 1987 169–173.
- Forsberg, L., 1985. Site variability and settlement patterns: An analysis of the hunter-gatherer settlement system in the Lule River Valley, 1500 B.C.-B.C./A.D. Department of Archaeology. Umeå University, Umeå.
- Gattiglia, G., 2015. Think big about data: Archaeology and the Big Data challenge. *Archäologische Informationen* 38, 113–124. <https://doi.org/10.11588/ai.2015.1.26155>
- Gawęda, A., Cebulak, S., 1999. The origin of graphite in the crystalline basement of the Western Tatra Mountains (Western Carpathians, S-Poland). *Geologica Carpathica* 50, 295–303.
- Geladi, P., Linderholm, J., 2020. 2.03 - Principal Component Analysis , in: Brown, S., Tauler, R., Walczak, B. (Eds.), Comprehensive Chemometrics (Second Edition). Elsevier, Oxford, pp. 17–37. <https://doi.org/10.1016/B978-0-12-409547-2.14892-9>
- Geologiska Föreningen i Stockholm, 1925. Mötet den 5 februari 1925. *Geologiska Föreningen i Stockholm Förhandlingar* 47, 145–154. <https://doi.org/10.1080/11035892509443187>
- Gillet, P., Le Cléac'h, A., Madon, M., 1990. High-temperature raman spectroscopy of SiO₂ and GeO₂ Polymorphs: Anharmonicity and thermodynamic properties at high-temperatures. *Journal of Geophysical Research: Solid Earth* 95, 21635–21655. <https://doi.org/10.1029/JB095iB13p21635>
- Grunsky, E.C., Caritat, P. de, 2020. State-of-the-art analysis of geochemical data for mineral exploration. *Geochemistry: Exploration, Environment, Analysis* 20, 217–232. <https://doi.org/10.1144/geochem2019-031>
- Halén, O., 1994. Sedentariness during the Stone Age of Northern Sweden : In the light of the Alträsket site, c. 5000 B.C., and the Comb Ware site Lillberget, c. 3900 B.C. : Source critical problems of representativity in archaeology, *Acta archaeologica Lundensia. Series in 4o,*.
- Hall, E.T., 1960. X-RAY FLUORESCENT ANALYSIS APPLIED TO ARCHAEOLOGY. *Archaeometry* 3, 29–35. <https://doi.org/10.1111/j.1475-4754.1960.tb00514.x>
- Hanson, B.A., 2016. ChemoSpec: Exploratory Chemometrics for Spectroscopy.
- Hazen, R.M., Morrison, S.M., 2022. On the paragenetic modes of minerals: A mineral evolution perspective. *American Mineralogist* 107, 1262–1287. <https://doi.org/10.2138/am-2022-8099>
- Holm, L., 1991. The use of stone and hunting of reindeer a study of stone tool manufacture and hunting of large mammals in the central Scandes c. 6000-1 BC, Archaeology and environment. Dept. of Archaeology [Institutionen för arkeologi], Umeå University, Umeå.
- Howard, J.L., 2005. The Quartzite Problem Revisited. *The Journal of Geology* 113, 707–713. <https://doi.org/10.1086/449328>
- Hunt, G.R., 1977. Spectral signatures of particular minerals in the visible and near infrared.

- Geophysics 42, 501–513.
- Käck, J., 2009. Samlingsboplatser? : En diskussion om mänskors möten i norr 7000 f kr-kr f med särskild utgångspunkt i data från ställv... Institutionen för idé- och samhällsstudier, Umeå universitet, Umeå.
- Kloprogge, J.T., 2017. Chapter 6 - raman spectroscopy of clay minerals, in: Gates, W.P., Kloprogge, J.T., Madejová, J., Bergaya, F. (Eds.), Infrared and Raman Spectroscopies of Clay Minerals, Developments in Clay Science. Elsevier, pp. 150–199. <https://doi.org/10.1016/B978-0-08-100355-8.00006-0>
- Knight, R.D., Kjarsgaard, B.A., Russell, H.A.J., 2021. An analytical protocol for determining the elemental chemistry of Quaternary sediments using a portable X-ray fluorescence spectrometer. Applied Geochemistry 131, 105026. <https://doi.org/10.1016/j.apgeochem.2021.105026>
- Knutsson, H., Knutsson, K., Molin, F., Zetterlund, P., 2016. From flint to quartz: Organization of lithic technology in relation to raw material availability during the pioneer process of Scandinavia. Quaternary International 424, 32–57. <https://doi.org/10.1016/j.quaint.2015.10.062>
- Lee, A.Y., Yang, K., Anh, N.D., Park, C., Lee, S.M., Lee, T.G., Jeong, M.S., 2021. Raman study of D* band in graphene oxide and its correlation with reduction. Applied Surface Science 536, 147990. <https://doi.org/10.1016/j.apsusc.2020.147990>
- Lieber, C.A., Mahadevan-Jansen, A., 2003. Automated Method for Subtraction of Fluorescence from Biological Raman Spectra. Appl Spectrosc 57, 1363–1367. <https://doi.org/10.1366/000370203322554518>
- Linderholm, J., Geladi, P., 2014a. Portable near infrared spectroscopy and imaging on archaeological sites and samples in the MOBIMA project. Part 1. Field spectroscopy. NIR news 25, 11–15. <https://doi.org/10.1255/nirn.1457>
- Linderholm, J., Geladi, P., 2014b. Portable near infrared spectroscopy and imaging on archaeological sites and samples in the MOBIMA project. Part 2. The potential of hyperspectral field imaging. NIR news 25, 8–12.
- Lundberg, Å., 1997. Vinterbyar : Ett bandsamhälles territorier i norrlands inland, 4500-2500 f. Kr. = winter villages : The territori... Arkeologiska institutionen, Univ., Umeå.
- Lundblad, S.P., Mills, P.R., Hon, K., 2008. ANALYSING ARCHAEOLOGICAL BASALT USING NON-DESTRUCTIVE ENERGY-DISPERSIVE x-RAY FLUORESCENCE (EDXRF): EFFECTS OF POST-DEPOSITIONAL CHEMICAL WEATHERING AND SAMPLE SIZE ON ANALYTICAL PRECISION*. Archaeometry 50, 1–11. <https://doi.org/https://doi.org/10.1111/j.1475-4754.2007.00345.x>
- Mark, Howard., Workman, Jr., Jerry, 2021. Chemometrics in Spectroscopy : Revised Second Edition., 2nd ed. ed, Chemometrics in Spectroscopy. Elsevier Science & Technology, San Diego.
- Menne, J., Holzheid, A., Heilmann, C., 2020. Multi-scale measurements of neolithic ceramics—a methodological comparison of portable energy-dispersive XRF, wavelength-dispersive XRF, and microcomputer tomography. Minerals 10, 931. <https://doi.org/10.3390/min10100931>
- Mishra, P., Roger, J.-M., Jouan-Rimbaud-Bouveresse, D., Biancolillo, A., Marini, F., Nordon, A., Rutledge, D.N., 2021. Recent trends in multi-block data analysis in chemometrics for multi-source data integration. TrAC Trends in Analytical Chemistry 137, 116206. <https://doi.org/10.1016/j.trac.2021.116206>
- Mjærum, A., 2012. The bifacial arrowheads in Southeast Norway. A chronological study. Acta Archaeologica 83, 105–143.
- Nafie, L.A., 2001. Theory of Raman Scattering, in: Lewis, I.R., Edwards, H.G.M. (Eds.), Handbook of Raman Spectroscopy : From the Research Laboratory to the Process Line. Marcel Dekker, New York, pp. 1–10.

- Norris, K.H., 1996. History of NIR. *Journal of near infrared spectroscopy* (United Kingdom) 4, 31–37. <https://doi.org/10.1255/jnirs.941>
- Osborne, B.G., Hindle, P.H., Fearn, T., 1993. Practical NIR spectroscopy : With applications in food and beverage analysis, 2. ed. ed. Longman Scientific & Technical, Harlow.
- Palarea-Albaladejo, J., Martin-Fernandez, J., 2015. [zCompositions – r package for multivariate imputation of left-censored data under a compositional approach](#). *Chemometrics and Intelligent Laboratory Systems* 143, 85–96.
- Pawlowsky-Glahn, V., Egozcue, J.J., 2006. Compositional data and their analysis: An introduction. Geological Society, London, Special Publications 264, 1–10. <https://doi.org/10.1144/GSL.SP.2006.264.01.01>
- Pawlowsky-Glahn, V., Egozcue, J.J., Tolosana-Delgado, R., 2015. Modeling and Analysis of Compositional Data. John Wiley & Sons, Chichester, UK.
- Pimenta, M.A., Dresselhaus, G., Dresselhaus, M.S., Cançado, L.G., Jorio, A., Saito, R., 2007. Studying disorder in graphite-based systems by Raman spectroscopy. *Phys. Chem. Chem. Phys.* 9, 1276–1290. <https://doi.org/10.1039/B613962K>
- Prieto, A., Yusta, I., Arrizabalaga, A., 2020. From petrographic analysis to stereomicroscopic characterisation: A geoarchaeological approach to identify quartzite artefacts in the Cantabrian Region. *Archaeological and Anthropological Sciences* 12, 32. <https://doi.org/10.1007/s12520-019-00981-7>
- Prieto, A., Yusta, I., Arrizabalaga, A., 2019. Defining and Characterizing Archaeological Quartzite: Sedimentary and Metamorphic Processes in the Lithic Assemblages of El Habario and El Arteu (Cantabrian Mountains, Northern Spain). *Archaeometry* 61, 14–30. <https://doi.org/10.1111/arcm.12397>
- Prieto, A., Yusta, I., García-Rojas, M., Arrizabalaga, A., Baena Preysler, J., 2021. Quartzite procurement in conglomerates and deposits: Geoarchaeological characterization of potential catchment areas in the central part of the Cantabrian Region, Spain. *GEOARCHAEOLOGY* 36, 490–510. <https://doi.org/10.1002/gea.21838>
- R Core Team, 2021a. R: A language and environment for statistical computing.
- R Core Team, 2021b. Prcomp function - RDocumentation [WWW Document]. URL <https://www.rdocumentation.org/packages/stats/versions/3.6.2/topics/prcomp> (accessed 10.18.2021).
- Ramacciotti, M., Gallelo, G., Pastor, A., Diez Castillo, A., García Puchol, O., 2019. Chert Nucleus and Cortex Characterization for Archaeological Provenance Study Tested in the Prebaetic System Region (Valencian Community, Spain). *LITHIC TECHNOL* 44, 166–180. <https://doi.org/10.1080/01977261.2019.1618043>
- Ramanaidou, E., Wells, M., Lau, I., Laukamp, C., 2015. Characterization of iron ore by visible and infrared reflectance and,raman spectroscopies, in: Lu, L. (Ed.), Iron Ore. Woodhead Publishing, pp. 191–228. <https://doi.org/https://doi.org/10.1016/B978-1-78242-156-6.00006-X>
- Rankama, T., Manninen, M.A., Hertell, E., Tallavaara, M., 2006. Simple production and social strategies: Do they meet? Social dimensions in Eastern Fennoscandian quartz, in: Apel, J., Knutsson, K. (Eds.), Skilled Production and Social Reproduction : Aspects of Traditional Stone-Tool Technologies : Proceedings of a Symposium in Uppsala, August 20-24, 2003, SAU Stone Studies. *Societas archaeologica Upsaliensis*, Uppsala.
- Reimann, C., Filzmoser, P., Fabian, K., Hron, K., Birke, M., Demetriadis, A., Dinelli, E., Ladenberger, A., 2012. The concept of compositional data analysis in practice — total major element concentrations in agricultural and grazing land soils of europe. *Science of The Total Environment* 426, 196–210. <https://doi.org/https://doi.org/10.1016/j.scitotenv.2012.02.032>
- Schmid, M., Rath, D., Diebold, U., 2022. Why and How Savitzky–Golay Filters Should Be Replaced. *ACS Meas. Au* 2, 185–196. <https://doi.org/10.1021/acsmeasuresciau.1c00054>

- Sciuto, C., 2018. Carved Mountains and Moving Stones - Applications of Near Infrared Spectroscopy for Mineral Characterisation in Provenance Studies. Department of Historical, Philosophical and Religious Studies. Umeå University, Umeå.
- Sciuto, C., Geladi, P., La Rosa, L., Linderholm, J., Thyrel, M., 2019. Hyperspectral Imaging for Characterization of Lithic Raw Materials: The Case of a Mesolithic Dwelling in Northern Sweden. *Lithic Technology* 44, 22–35. <https://doi.org/10.1080/01977261.2018.1543105>
- Shackley, M.S., 2011a. X-ray fluorescence spectrometry (XRF) in geoarchaeology. New York : Springer, New York.
- Shackley, M.S., 2011b. An introduction to x-ray fluorescence (XRF) in archaeology. New York : Springer, New York.
- Sitko, R., Zawisza, B., 2012. Quantification in x-ray fluorescence spectrometry, in: Sharma, S.K. (Ed.), X-Ray Spectroscopy. IntechOpen, Rijeka. <https://doi.org/https://doi.org/10.5772/29367>
- Skolnick, H., 1965. The quartzite problem. *Journal of Sedimentary Research* 35, 12–21. <https://doi.org/10.1306/74D711E0-2B21-11D7-8648000102C1865D>
- Smith, D.C., Carabatos-Nédelec, C., 2001. Raman Spectroscopy Applied to Crystals: Phenomena and Principles, Concepts and Conventions, in: Lewis, I.R., Edwards, H.G.M. (Eds.), *Handbook of Raman Spectroscopy: From the Research Laboratory to the Process Line*. Marcel Dekker, New York, pp. 349–423.
- Stephens, M.B., Bergman Weihed, J., 2020. Sweden: Lithotectonic framework, tectonic evolution and mineral resources, Geological Society Memoir. The Geological Society of London, London.
- Stroeven, A.P., Hätteström, C., Kleiman, J., Heyman, J., Fabel, D., Fredin, O., Goodfellow, B.W., Harbor, J.M., Jansen, J.D., Olsen, L., Caffee, M.W., Fink, D., Lundqvist, J., Rosqvist, G.C., Strömberg, B., Jansson, K.N., 2016. Deglaciation of Fennoscandia. *Quaternary Science Reviews* 147, 91–121. <https://doi.org/10.1016/j.quascirev.2015.09.016>
- Tallavaara, M., Manninen, M.A., Hertell, E., Rankama, T., 2010. How flakes shatter: A critical evaluation of quartz fracture analysis. *Journal of Archaeological Science* 37, 2442–2448. <https://doi.org/10.1016/j.jas.2010.05.005>
- Thermo Fisher Scientific, 2018. Niton XL5 Analyzer User's Guide.
- Trang, D., Lucey, P.G., Gillis-Davis, J.J., Cahill, J.T.S., Klima, R.L., Isaacson, P.J., 2013. Near-infrared optical constants of naturally occurring olivine and synthetic pyroxene as a function of mineral composition. *Journal of Geophysical Research: Planets* 118, 708–732. <https://doi.org/10.1002/jgre.20072>
- Tykot, R.H., 2017. Obsidian studies in the prehistoric central mediterranean: After 50 years, what have we learned and what still needs to be done? *Open Archaeology* 3, 264–278. <https://doi.org/doi:10.1515/opar-2017-0018>
- Tykot, R.H., 2003. Determining the source of lithic artifacts and reconstructing trade in the ancient world, in: Kardulias, N.P., Yerkes, R.W. (Eds.), *Written in Stone: The Multiple Dimensions of Lithic Analysis*. Lexington Books, Lanham, Md.
- Ukar, E., Cloos, M., 2016. Graphite-schist blocks in the Franciscan Mélange, San Simeon, California: Evidence of high-P metamorphism. *Journal of Metamorphic Geology* 34, 191–208. <https://doi.org/10.1111/jmg.12174>
- Vollebregt, S., Ishihara, R., Tichelaar, F.D., Hou, Y., Beenakker, C.I.M., 2012. Influence of the growth temperature on the first and second-order Raman band ratios and widths of carbon nanotubes and fibers. *Carbon* 50, 3542–3554. <https://doi.org/10.1016/j.carbon.2012.03.026>
- Zhong, X., Loges, A., Roddatis, V., John, T., 2021. Measurement of crystallographic orientation of quartz crystal using Raman spectroscopy: Application to entrapped inclusions. *Contributions*

to Mineralogy and Petrology 176, 89. <https://doi.org/10.1007/s00410-021-01845-x>

Colophon

This report was generated on 2023-09-13 12:36:51 using the following computational environment and dependencies:

```
#> - Session info -----
#>   setting  value
#>   version R version 4.2.2 (2022-10-31 ucrt)
#>   os        Windows 10 x64 (build 19045)
#>   system   x86_64, mingw32
#>   ui        RTerm
#>   language (EN)
#>   collate  English_Europe.utf8
#>   ctype    English_Europe.utf8
#>   tz       Europe/Berlin
#>   date     2023-09-13
#>   pandoc   3.1.1 @ C:/Program Files/RStudio/resources/app/bin/quarto/bin/tools/ (via rmarkdown)
#>
#> - Packages -----
#>   ! package          * version  date (UTC) lib source
#>   P abind            1.4-5     2016-07-21 [?] CRAN (R 4.2.0)
#>   P askpass           1.2.0     2023-09-03 [?] CRAN (R 4.2.3)
#>   P backports         1.4.1     2021-12-13 [?] CRAN (R 4.2.0)
#>   P baseline          1.3-4     2022-07-06 [?] CRAN (R 4.2.3)
#>   P bitops             1.0-7     2021-04-24 [?] CRAN (R 4.2.0)
#>   P boot              1.3-28    2021-05-03 [?] CRAN (R 4.2.2)
#>   P broom             1.0.5     2023-06-09 [?] CRAN (R 4.2.3)
#>   P cachem            1.0.8     2023-05-01 [?] CRAN (R 4.2.3)
#>   P callr              3.7.3     2022-11-02 [?] CRAN (R 4.2.2)
#>   P car               3.1-2     2023-03-30 [?] CRAN (R 4.2.3)
#>   P carData            3.0-5     2022-01-06 [?] CRAN (R 4.2.2)
#>   P ChemoSpec          * 6.1.9    2023-06-07 [?] CRAN (R 4.2.3)
#>   P ChemoSpecUtils     * 1.0.3    2023-05-30 [?] CRAN (R 4.2.3)
#>   P class              7.3-20    2022-01-16 [?] CRAN (R 4.2.2)
#>   P cli                3.6.1     2023-03-23 [?] CRAN (R 4.2.3)
#>   P cluster             2.1.4     2022-08-22 [?] CRAN (R 4.2.2)
#>   P codetools           0.2-18    2020-11-04 [?] CRAN (R 4.2.2)
#>   P colorspace          2.1-0     2023-01-23 [?] CRAN (R 4.2.2)
#>   P commonmark          1.9.0     2023-03-17 [?] CRAN (R 4.2.3)
#>   P cowplot             * 1.1.1    2020-12-30 [?] CRAN (R 4.2.2)
#>   P crayon              1.5.2     2022-09-29 [?] CRAN (R 4.2.2)
#>   P crul                1.4.0     2023-05-17 [?] CRAN (R 4.2.3)
#>   P curl                5.0.2     2023-08-14 [?] CRAN (R 4.2.3)
#>   P cvTools              0.3.2     2012-05-14 [?] CRAN (R 4.2.3)
#>   P data.table           * 1.14.8   2023-02-17 [?] CRAN (R 4.2.2)
#>   P DEoptimR              1.1-2     2023-08-28 [?] CRAN (R 4.2.3)
#>   P deSolve              1.38      2023-09-05 [?] CRAN (R 4.2.3)
```

#> P devtools	2.4.5	2022-10-11	[?]	CRAN	(R 4.2.2)
#> P digest	0.6.33	2023-07-07	[?]	CRAN	(R 4.2.3)
#> P diptest	0.76-0	2021-05-04	[?]	CRAN	(R 4.2.0)
#> P dplyr	* 1.1.3	2023-09-03	[?]	CRAN	(R 4.2.3)
#> P e1071	1.7-13	2023-02-01	[?]	CRAN	(R 4.2.2)
#> P ellipsis	0.3.2	2021-04-29	[?]	CRAN	(R 4.2.2)
#> P evaluate	0.21	2023-05-05	[?]	CRAN	(R 4.2.3)
#> P factoextra	* 1.0.7	2020-04-01	[?]	CRAN	(R 4.2.3)
#> P fansi	1.0.4	2023-01-22	[?]	CRAN	(R 4.2.3)
#> P farver	2.1.1	2022-07-06	[?]	CRAN	(R 4.2.2)
#> P fastmap	1.1.1	2023-02-24	[?]	CRAN	(R 4.2.3)
#> P fda	6.1.4	2023-05-23	[?]	CRAN	(R 4.2.3)
#> P fds	1.8	2018-10-31	[?]	CRAN	(R 4.2.3)
#> P flexmix	2.3-19	2023-03-16	[?]	CRAN	(R 4.2.3)
#> P flextable	* 0.9.3	2023-09-07	[?]	CRAN	(R 4.2.3)
#> P fontBitstreamVera	0.1.1	2017-02-01	[?]	CRAN	(R 4.2.0)
#> P fontLiberation	0.1.0	2016-10-15	[?]	CRAN	(R 4.2.0)
#> P fontquiver	0.2.1	2017-02-01	[?]	CRAN	(R 4.2.3)
#> Pforcats	* 1.0.0	2023-01-29	[?]	CRAN	(R 4.2.2)
#> P foreach	1.5.2	2022-02-02	[?]	CRAN	(R 4.2.3)
#> P fpc	2.2-10	2023-01-07	[?]	CRAN	(R 4.2.3)
#> P fs	1.6.3	2023-07-20	[?]	CRAN	(R 4.2.3)
#> P gdtools	0.3.3	2023-03-27	[?]	CRAN	(R 4.2.3)
#> P generics	0.1.3	2022-07-05	[?]	CRAN	(R 4.2.2)
#> P gfonts	0.2.0	2023-01-08	[?]	CRAN	(R 4.2.3)
#> P GGally	2.1.2	2021-06-21	[?]	CRAN	(R 4.2.3)
#> P ggfortify	0.4.16	2023-03-20	[?]	CRAN	(R 4.2.3)
#> P ggnewscale	0.4.9	2023-05-25	[?]	CRAN	(R 4.2.3)
#> P ggplot2	* 3.4.3	2023-08-14	[?]	CRAN	(R 4.2.3)
#> P ggpubfigs	0.0.1	2023-09-11	[1]	Github	(JLSteenwyk/ggpubfigs@264716c)
#> P ggpubr	* 0.6.0	2023-02-10	[?]	CRAN	(R 4.2.2)
#> P ggrepel	0.9.3	2023-02-03	[?]	CRAN	(R 4.2.2)
#> P ggsignif	0.6.4	2022-10-13	[?]	CRAN	(R 4.2.2)
#> P ggttext	* 0.1.2	2022-09-16	[?]	CRAN	(R 4.2.3)
#> P glue	1.6.2	2022-02-24	[?]	CRAN	(R 4.2.2)
#> P gridBase	* 0.4-7	2014-02-24	[?]	CRAN	(R 4.2.3)
#> P gridExtra	2.3	2017-09-09	[?]	CRAN	(R 4.2.2)
#> P gridtext	0.1.5	2022-09-16	[?]	CRAN	(R 4.2.3)
#> P gtable	0.3.4	2023-08-21	[?]	CRAN	(R 4.2.3)
#> P hdrcde	3.4	2021-01-18	[?]	CRAN	(R 4.2.3)
#> P here	1.0.1	2020-12-13	[?]	CRAN	(R 4.2.2)
#> P hms	1.1.3	2023-03-21	[?]	CRAN	(R 4.2.3)
#> P htmltools	0.5.6	2023-08-10	[?]	CRAN	(R 4.2.3)
#> P htmlwidgets	1.6.2	2023-03-17	[?]	CRAN	(R 4.2.3)
#> P httpcode	0.3.0	2020-04-10	[?]	CRAN	(R 4.2.3)
#> P httpuv	1.6.11	2023-05-11	[?]	CRAN	(R 4.2.3)
#> P httr	1.4.7	2023-08-15	[?]	CRAN	(R 4.2.3)
#> P insight	0.19.4	2023-09-10	[?]	CRAN	(R 4.2.2)

#> P iterators	1.0.14	2022-02-05	[?]	CRAN	(R 4.2.3)
#> P jsonlite	1.8.7	2023-06-29	[?]	CRAN	(R 4.2.3)
#> P kernlab	0.9-32	2023-01-31	[?]	CRAN	(R 4.2.2)
#> P KernSmooth	2.23-20	2021-05-03	[?]	CRAN	(R 4.2.2)
#> P knitr	1.43	2023-05-25	[?]	CRAN	(R 4.2.3)
#> P ks	1.14.1	2023-08-10	[?]	CRAN	(R 4.2.3)
#> P labeling	0.4.3	2023-08-29	[?]	CRAN	(R 4.2.3)
#> P laeken	0.5.2	2021-10-06	[?]	CRAN	(R 4.2.3)
#> P later	1.3.1	2023-05-02	[?]	CRAN	(R 4.2.3)
#> P lattice	0.20-45	2021-09-22	[?]	CRAN	(R 4.2.2)
#> P lazyeval	0.2.2	2019-03-15	[?]	CRAN	(R 4.2.3)
#> P lifecycle	1.0.3	2022-10-07	[?]	CRAN	(R 4.2.2)
#> P limSolve	1.5.6	2019-11-14	[?]	CRAN	(R 4.2.3)
#> P lmtest	0.9-40	2022-03-21	[?]	CRAN	(R 4.2.3)
#> P loder	* 0.2.1	2022-12-16	[?]	CRAN	(R 4.2.3)
#> P lpSolve	5.6.18	2023-02-01	[?]	CRAN	(R 4.2.2)
#> P lubridate	* 1.9.2	2023-02-10	[?]	CRAN	(R 4.2.2)
#> P magick	2.7.5	2023-08-07	[?]	CRAN	(R 4.2.3)
#> P magrittr	2.0.3	2022-03-30	[?]	CRAN	(R 4.2.2)
#> P markdown	1.8	2023-08-23	[?]	CRAN	(R 4.2.3)
#> P MASS	7.3-60	2023-05-04	[?]	CRAN	(R 4.2.3)
#> P mathjaxr	1.6-0	2022-02-28	[?]	CRAN	(R 4.2.3)
#> P Matrix	1.5-1	2022-09-13	[?]	CRAN	(R 4.2.2)
#> P mclust	6.0.0	2022-10-31	[?]	CRAN	(R 4.2.3)
#> P memoise	2.0.1	2021-11-26	[?]	CRAN	(R 4.2.2)
#> P mime	0.12	2021-09-28	[?]	CRAN	(R 4.2.0)
#> P miniUI	0.1.1.1	2018-05-18	[?]	CRAN	(R 4.2.2)
#> P modeltools	0.2-23	2020-03-05	[?]	CRAN	(R 4.2.0)
#> P munsell	0.5.0	2018-06-12	[?]	CRAN	(R 4.2.2)
#> P mvtnorm	1.2-3	2023-08-25	[?]	CRAN	(R 4.2.3)
#> P NADA	1.6-1.1	2020-03-22	[?]	CRAN	(R 4.2.3)
#> P nnet	7.3-18	2022-09-28	[?]	CRAN	(R 4.2.2)
#> P officedown	* 0.3.1	2023-09-02	[?]	CRAN	(R 4.2.3)
#> P officer	* 0.6.2	2023-03-28	[?]	CRAN	(R 4.2.3)
#> P openssl	2.1.0	2023-07-15	[?]	CRAN	(R 4.2.3)
#> P patchwork	1.1.3	2023-08-14	[?]	CRAN	(R 4.2.3)
#> P pcaPP	2.0-3	2022-10-24	[?]	CRAN	(R 4.2.3)
#> P perry	0.3.1	2021-11-03	[?]	CRAN	(R 4.2.3)
#> P pillar	1.9.0	2023-03-22	[?]	CRAN	(R 4.2.3)
#> P pkgbuild	1.4.2	2023-06-26	[?]	CRAN	(R 4.2.3)
#> P pkgconfig	2.0.3	2019-09-22	[?]	CRAN	(R 4.2.2)
#> P pkgload	1.3.2.1	2023-07-08	[?]	CRAN	(R 4.2.3)
#> P plotly	4.10.2	2023-06-03	[?]	CRAN	(R 4.2.3)
#> P pls	* 2.8-2	2023-05-19	[?]	CRAN	(R 4.2.3)
#> P plyr	1.8.8	2022-11-11	[?]	CRAN	(R 4.2.2)
#> P png	* 0.1-8	2022-11-29	[?]	CRAN	(R 4.2.2)
#> P prabclus	2.3-2	2020-01-08	[?]	CRAN	(R 4.2.3)
#> P pracma	2.4.2	2022-09-22	[?]	CRAN	(R 4.2.3)

#> P prettyunits	1.1.1	2020-01-24	[?]	CRAN	(R 4.2.2)
#> P processx	3.8.2	2023-06-30	[?]	CRAN	(R 4.2.3)
#> P profvis	0.3.8	2023-05-02	[?]	CRAN	(R 4.2.3)
#> P promises	1.2.1	2023-08-10	[?]	CRAN	(R 4.2.3)
#> P prospectr	* 0.2.6	2022-08-31	[?]	CRAN	(R 4.2.3)
#> P proxy	0.4-27	2022-06-09	[?]	CRAN	(R 4.2.2)
#> P ps	1.7.5	2023-04-18	[?]	CRAN	(R 4.2.3)
#> P purrr	* 1.0.2	2023-08-10	[?]	CRAN	(R 4.2.3)
#> P quadprog	1.5-8	2019-11-20	[?]	CRAN	(R 4.2.0)
#> P R.methodsS3	1.8.2	2022-06-13	[?]	CRAN	(R 4.2.2)
#> P R.oo	1.25.0	2022-06-12	[?]	CRAN	(R 4.2.2)
#> P R.utils	2.12.2	2022-11-11	[?]	CRAN	(R 4.2.3)
#> P R6	2.5.1	2021-08-19	[?]	CRAN	(R 4.2.2)
#> P ragg	1.2.5	2023-01-12	[?]	CRAN	(R 4.2.2)
#> P rainbow	3.7	2022-10-09	[?]	CRAN	(R 4.2.3)
#> P ranger	0.15.1	2023-04-03	[?]	CRAN	(R 4.2.3)
#> P RColorBrewer	1.1-3	2022-04-03	[?]	CRAN	(R 4.2.0)
#> P Rcpp	1.0.11	2023-07-06	[?]	CRAN	(R 4.2.3)
#> P RCurl	1.98-1.12	2023-03-27	[?]	CRAN	(R 4.2.3)
#> P readJDX	0.6.1	2021-09-20	[?]	CRAN	(R 4.2.3)
#> P readr	* 2.1.4	2023-02-10	[?]	CRAN	(R 4.2.2)
#> P remotes	2.4.2.1	2023-07-18	[?]	CRAN	(R 4.2.3)
#> P reshape	0.8.9	2022-04-12	[?]	CRAN	(R 4.2.3)
#> P reshape2	1.4.4	2020-04-09	[?]	CRAN	(R 4.2.3)
#> P rlang	1.1.1	2023-04-28	[?]	CRAN	(R 4.2.3)
#> P rmarkdown	2.24	2023-08-14	[?]	CRAN	(R 4.2.3)
#> P robCompositions	* 2.4.1	2023-08-25	[?]	CRAN	(R 4.2.3)
#> P robustbase	0.99-0	2023-06-16	[?]	CRAN	(R 4.2.3)
#> P robustHD	0.7.4	2023-01-18	[?]	CRAN	(R 4.2.3)
#> P rprojroot	2.0.3	2022-04-02	[?]	CRAN	(R 4.2.2)
#> P rrcov	1.7-4	2023-06-24	[?]	CRAN	(R 4.2.3)
#> P rstatix	0.7.2	2023-02-01	[?]	CRAN	(R 4.2.2)
#> P rstudioapi	0.15.0	2023-07-07	[?]	CRAN	(R 4.2.3)
#> P rvg	0.3.3	2023-05-10	[?]	CRAN	(R 4.2.3)
#> P scales	1.2.1	2022-08-20	[?]	CRAN	(R 4.2.2)
#> P see	0.8.0	2023-06-05	[?]	CRAN	(R 4.2.3)
#> P sessioninfo	1.2.2	2021-12-06	[?]	CRAN	(R 4.2.2)
#> P shiny	1.7.5	2023-08-12	[?]	CRAN	(R 4.2.3)
#> P shinyjs	2.1.0	2021-12-23	[?]	CRAN	(R 4.2.3)
#> P sp	2.0-0	2023-06-22	[?]	CRAN	(R 4.2.3)
#> P SparseM	1.81	2021-02-18	[?]	CRAN	(R 4.2.0)
#> P spectrolab	* 0.0.18	2023-02-12	[?]	CRAN	(R 4.2.3)
#> P stringi	1.7.12	2023-01-11	[?]	CRAN	(R 4.2.2)
#> P stringr	* 1.5.0	2022-12-02	[?]	CRAN	(R 4.2.2)
#> P survival	3.4-0	2022-08-09	[?]	CRAN	(R 4.2.2)
#> P systemfonts	1.0.4	2022-02-11	[?]	CRAN	(R 4.2.2)
#> P textshaping	0.3.6	2021-10-13	[?]	CRAN	(R 4.2.2)
#> P tibble	* 3.2.1	2023-03-20	[?]	CRAN	(R 4.2.3)

```

#> P tidyverse          * 1.3.0      2023-01-24 [?] CRAN (R 4.2.2)
#> P tidyselect         1.2.0       2022-10-10 [?] CRAN (R 4.2.2)
#> P tidyverse          * 2.0.0       2023-02-22 [?] CRAN (R 4.2.2)
#> P timechange         0.2.0       2023-01-11 [?] CRAN (R 4.2.2)
#> P truncnorm          1.0-9       2023-03-20 [?] CRAN (R 4.2.3)
#> P tzdb                0.4.0       2023-05-12 [?] CRAN (R 4.2.3)
#> P urlchecker         1.0.1       2021-11-30 [?] CRAN (R 4.2.2)
#> P usethis             2.2.2       2023-07-06 [?] CRAN (R 4.2.3)
#> P utf8                1.2.3       2023-01-31 [?] CRAN (R 4.2.3)
#> P uuid                1.1-1       2023-08-17 [?] CRAN (R 4.2.3)
#> P vcd                 1.4-11      2023-02-01 [?] CRAN (R 4.2.3)
#> P vctrs               0.6.3       2023-06-14 [?] CRAN (R 4.2.3)
#> P VIM                  6.2.2       2022-08-25 [?] CRAN (R 4.2.3)
#> P viridisLite         0.4.2       2023-05-02 [?] CRAN (R 4.2.3)
#> P withr               2.5.0       2022-03-03 [?] CRAN (R 4.2.2)
#> P xfun                 0.40        2023-08-09 [?] CRAN (R 4.2.3)
#> P xml2                 1.3.5       2023-07-06 [?] CRAN (R 4.2.3)
#> P xtable               1.8-4       2019-04-21 [?] CRAN (R 4.2.2)
#> P yaml                 2.3.7       2023-01-23 [?] CRAN (R 4.2.3)
#> P zCompositions        1.4.1       2023-08-23 [?] CRAN (R 4.2.3)
#> P zip                  2.3.0       2023-04-17 [?] CRAN (R 4.2.3)
#> P zoo                  1.8-12      2023-04-13 [?] CRAN (R 4.2.3)
#>
#> [1] C:/Users/sjola/AppData/Local/R/cache/R/renv/library/quartzite.complexities-ac41d908/R-
#> [2] C:/Users/sjola/AppData/Local/Temp/Rtmp4qEc7D/renv-system-library
#> [3] C:/Program Files/R/R-4.2.2/library
#>
#> P -- Loaded and on-disk path mismatch.
#>
#> -----

```

The current Git commit details are:

```

#> Local:    main C:/Users/sjola/Documents/VERSION CONTROL/quartzite.complexities
#> Remote:   main @ origin (https://github.com/MattiasSealander/quartzite.complexities.git)
#> Head:     [e74103c] 2023-09-13: Updated manuscript

```